

Raman gas sensing technology: A new horizon?

MAJUMDER, Deblina, JANANI, Ronak, SCRIMSHIRE, Alex <<http://orcid.org/0000-0002-6828-3620>>, STONE, Alex, BROOKS, William, HOLCROFT, Chris, WERNER, Rob, GREEN, Spencer, WHEELER, Natalie and BINGHAM, Paul <<http://orcid.org/0000-0001-6017-0798>>

Available from Sheffield Hallam University Research Archive (SHURA) at:

<https://shura.shu.ac.uk/35116/>

This document is the Published Version [VoR]

Citation:

MAJUMDER, Deblina, JANANI, Ronak, SCRIMSHIRE, Alex, STONE, Alex, BROOKS, William, HOLCROFT, Chris, WERNER, Rob, GREEN, Spencer, WHEELER, Natalie and BINGHAM, Paul (2025). Raman gas sensing technology: A new horizon? *Sensors and Actuators Reports*, 9: 100311. [Article]

Copyright and re-use policy

See <http://shura.shu.ac.uk/information.html>



Raman gas sensing technology: A new horizon?

Deblina Majumder^{a,b,*}, Ronak Janani^a, Alex Scrimshire^a, Alex Stone^a, William Brooks^c, Chris Holcroft^d, Rob Werner^d, Spencer Green^e, Natalie Wheeler^f, Paul . A . Bingham^a

^a Materials and Engineering Research Institute, Sheffield Hallam University, City Campus, Howard Street, Sheffield S1 1WB, United Kingdom

^b School of Engineering, Newcastle University, Newcastle upon Tyne NE1 7RU, United Kingdom

^c IS-Instruments, Pipers Business Centre, 220 Vale Rd, Tonbridge TN9 1SP, United Kingdom

^d Glass Technology Services, 9 Churchill Way, Chapelton, Sheffield, South Yorkshire S35 2PY, United Kingdom

^e Breedon Group, Pinnacle House, Breedon Quarry, Main Street, Breedon on the Hill, Derby DE73 8AP, United Kingdom

^f Optoelectronics Research Centre, University of Southampton, B53, West Highfield Campus, University Road, SO17 1BJ, United Kingdom

ARTICLE INFO

Keywords:

Raman spectroscopy
Gas sensors
Spontaneous
Stimulated
Coherent anti-stokes
Surface-enhanced
Tip-enhanced Raman scattering

ABSTRACT

The question in the title alludes to the importance of comprehending the relevance and manner of operation in the field of gas sensors, which is undeniably one of the most important scientific and economic interests. Despite being superior to several commonly used techniques, such as infrared (IR) spectroscopy, Nondispersive IR (NDIR) and gas chromatography coupled with mass spectrometry (GC-MS), Raman spectroscopy-based gas sensors are yet to be widely explored for real-world applications. Given the weak Raman effect, numerous innovative strategies have emerged to improve its utility in chemical sensing, biological imaging, and material characterization, among other applications. This review covers five important approaches with a high potential for use in Raman-based gas sensors: spontaneous (SRS), stimulated (StRS), coherent anti-Stokes (CARS), surface-enhanced (SERS), and tip-enhanced (TERS) Raman scattering spectroscopy. The initial strategy of this review is to provide the in-depth foundational knowledge necessary for the reader to grasp several types of Raman techniques, their advantages and limitations. This is followed by an overview of current competing technologies and their applications. The remainder of the paper focuses on recent major experimental findings based on the Raman techniques and their practical applications. As a comprehensive introduction to Raman spectroscopy, this review article also serves as a knowledge base for future developments in the field of gas sensors.

1. Introduction

Since the early 1900s, spectroscopic techniques in the field of gas sensing have been evolving, with infrared, ultraviolet, and visible light at the forefront of these advancements. These types of radiations were investigated for detection of hydrogen for uses in astrophysics as early as 1912. These wavelengths of radiation are used separately in several disciplines of gas sensing, from electronic noses to environmental monitoring [1–14]. Raman established Raman spectroscopy as a technique in the 1920s, drawing parallels between the known X-ray scattering Compton effect and radiation at, or near, visible wavelengths noting that the two should react similarly, with one type representing the optical mode of the molecule and the other the excited state [15]. He allegedly detected Raman light scattered from liquids such as benzene, but due to the limited sensitivity for quantifying gases, this technique remained a solid and liquid state technique for many years, with most of

its uses in investigating organic and crystalline materials [16,17]. Solid state Raman spectroscopy of minerals, for example, has become a method for identifying calcite and diamond carbon [18]. Rasetti's 1932 study involved gas identification utilising pressured systems to overcome limited sensitivity and achieve a representative signal [19]. Following this, a series of comparable proof-of-concept tests by multiple researchers demonstrated that Raman intensity was attainable for hydrogen, oxygen, nitrogen, simple volatile organics, nitrogen oxides, and carbon [20–25]. Previously, it was shown that absorption spectroscopies such as infrared (IR) are incapable of detecting homonuclear diatomic molecules [26]. This remained a hurdle until the introduction of high-power lasers in the 1960s, when Weber et al. proposed samples with lower pressure for nitrogen, oxygen, methylacetylene, and carbon dioxide samples [27]. After the rise in resolution that laser Raman spectroscopy cleared the path for gas sensing from other techniques, the research scene and market were yet pioneered. Because of the

* Corresponding author.

E-mail address: Deblina.Majumder@newcastle.ac.uk (D. Majumder).

convenience of sampling and excellent resolution without requiring enormous technological improvements, infrared, UV-vis, and gas chromatography coupled with mass spectrometry (GC-MS) have gained more interest. Raman effect on the other hand is very weak [20]. This means that any interferences are often stronger than the scattering signal itself, making background difficult to account for. One of the most significant influences is fluorescence which can overwhelm Raman scattering [28]. This remains an issue in modern Raman spectrometers, but new strategies, such as the use of optical fibres, have been developed to minimise this issue and increase signal-to-noise ratio. Infrared spectroscopy is a complementary technique to Raman and is one of its key competitors in the field of gas sensing. For decades, Fourier transform infrared spectroscopy (FTIR) has been utilised in environmental emission testing to detect combustion gases, ozone, and volatile hydrocarbons [29,30]. It also has the advantage of being more portable and running hot/wet due to the simplicity of the equipment. However, presence of water or moisture can at times be problematic since O–H bond has a strong and broad absorbance band in the IR spectrum above 3000 cm^{-1} and might cause some interference [28]. Furthermore, for a diatomic molecule to be IR active, it must be heteronuclear, which can be limiting for certain gases including H_2 , O_2 , N_2 , etc. In the 1950s, GC-MS was developed primarily as a tabletop technique of volatile compound analysis and is now often used for organic identification [31]. It employs a hollow column of wire covered with a polar substance through which the gas flows. The gas is then split out due to its polarizability, and its chemical makeup is determined by atomic weight within the mass spectrometer. While there are a few portable gas chromatograph units on the market, they are more popular as laboratory-based systems due to vibration sensitivity and lower selectivity for specific analytes [32]. Raman spectroscopy is a fairly selective technique that is capable of detecting homonuclear diatomic analytes. Thus, Raman spectroscopy has the potential to be a frontrunner commercial gas analysing system if modified to overcome its fluorescence and sensitivity shortcomings.

2. Contemporary competitors of gas Raman technique

Spectroscopy-based techniques always remain a challenging research area, even though they are commonly used for gas sensing. IR-based methods, such as direct infrared absorption spectroscopy [33–35], photoacoustic spectroscopy [36–38], or cavity ring-down spectroscopy [39], provide tremendous sensitivity due to the presence of higher absorption cross sections. However, these methods are unable to detect homonuclear diatomic molecules several of which are of high importance in a variety of disciplines, such as biological detections, environmental emissions, energy resources, and industrial processes [40–42], etc. Although a variety of gas analysis systems are now available, many more are in the works. Despite the availability of simultaneous multi-gas monitoring systems, some of the more specific pollutants, such as carbon monoxide, lead, nitrogen oxides, ground-level ozone, particle pollution, and so on, necessitate a specialised detection technique based on spectroscopic properties. Because of its exceptional sensitivity and selectivity, gas chromatography is one of the most widely used analytical techniques [43–45]. Some of the main limitations of this technique [46, 47] are relatively long measurement intervals and time-consuming sample pre-treatment processes, which limit its widespread applicability in many industrial sectors. Portable FTIR instruments are commonly used for industrial off-gas emission monitoring because they concurrently scan the entire mid-infrared range and using the appropriate software, the amount of each analyte can be estimated based on the distinctive absorptions [48–50]. Commercially available IR-based gas sensors include the GT5000 Terra [51], DX4015 [52], and GASEX AR Coptix S.A45 [53–55]. In addition to the aforementioned constraints in detection, environmental conditions characterised by elevated levels of humidity, dust, and corrosive agents pose challenges to the maintenance of infrared (IR) detectors, consequently escalating associated expenses [56].

NDIR, akin to FTIR, operates on the principle of infrared absorption by molecules at their distinctive frequencies. In this method, infrared radiation is transmitted through the molecules under examination, eliciting an IR spectrum characterized by the quantification of absorbed incident radiation at predetermined energy levels [3,8,14]. This technique is widely used for the detection of important air pollutants, such as CO , CO_2 , SO_2 , NO_x , N_2O , NH_3 , HCl , HF , CH_4 , etc [57]. Spectral selectivity in NDIR system is achieved by placing the appropriate filters before the detector [58]. For this reason, simultaneous detection of multiple target analytes increases complexity of analysis and the associated cost and operating time to a great extent [10,11]. The SIPROCESS GA700 (the latest generation of continuous process gas analytics) and Thermo Scientific™ 410i Carbon Dioxide Gas Analyser are examples of the currently used NDIR analysers for industrial off-gas emission monitoring purpose [12]. NDIR sensing, provided by companies like Senseair [61–63] (e.g., S8) and Edinburgh Sensors (e.g., Gascard NG) [59–67], relies on the absorption of infrared radiation by gas molecules. It offers high sensitivity, stability, and reliability, making it ideal for detecting various gases including CO_2 , methane, and volatile organic compounds (VOCs). Major advantages of this technique are its low energy consumption compared to other spectroscopic techniques [13] and its reliable detection of gaseous species over a broad concentration range. Because this method, like FTIR, can only identify analytes that absorb IR light, species like oxygen, hydrogen, and nitrogen cannot be identified using NDIR. In addition, the precision of detection for gases such as methane decreases when there are a number of different hydrocarbons present at the same time. The fact that the NDIR's operating principle is temperature dependent in addition to the fact that it is a costly technique, have limited its adoption for many actual field purposes. To analyse a wide variety of gases, some popular analysis systems combine many analytical methods into a single platform. As an example, the Horiba PG-350 is a portable multigas analyser that was developed by Horiba [68] is capable of monitoring NO_x , O_2 , SO_4 , CO_2 , and CO . This system uses chemiluminescence to measure the concentration of NO_x , NDIR to calculate the concentration of $\text{SO}_2/\text{CO}/\text{CO}_2$, and paramagnetic analysis to estimate the concentration of O_2 . Techniques such as electrochemical cells, zirconia cells, and FTIR are utilised by other types of systems [69]. Because of their dependability and portability, these systems are a popular choice among a variety of private testing organisations as well as establishments that perform continuous emission monitoring on-site.

However, these systems are not adaptable to new analytes and can only monitor the compounds they were built for. Because of this, other approaches need to be utilised in parallel to monitor a new analyte. Analysers for gases and liquids that are multi-component, customisable, and certified for use in hazardous environments include the Protea 2000 In-Situ CEM [70,71]. This kit can monitor up to six gaseous analytes, such as, CO_2 , CO , NH_3 , CH_4 , NO , NO_2 , N_2O , SO_2 , HCl , and H_2O . Due to selective wavelength irradiation, this widely installed in-situ analyser (reportedly over 4000 worldwide; compliant with international standards such as EN14181 and US EPA 40 cfr Part 60 & 75) [72] lacks cross sensitivity and is unable to provide any detail about any unknown analytes present in the sample. Examples of other available portable multigas analysers are: Dräger X-zone® 550057 [73], Flue gas analyser MIR 9000H IS ENVA58 and Gasmeter DX401559 [6,51,52]. Surface Plasmon Resonance (SPR) provides the advantage of detecting gas molecules without the need for labels and in real-time, by observing alterations in refractive index close to a metal surface, it falls short in terms of the precision and sensitivity that Raman spectroscopy gives [74]. SPR sensors have a main limitation in that they can only detect significant changes in refractive index, which makes them less appropriate for distinguishing between different types of gases or correctly detecting gases in trace level. Optical sensing techniques such as cavity-enhanced absorption spectroscopy (CEAS) [75] and photoacoustic spectroscopy (PAS) [74] provide excellent sensitivity and selectivity. However, they may be hindered by drawbacks such as

complexity, high cost, and vulnerability to external influence. SPR sensing, offered by Biosensing Instrument (e.g., SPRm 200™ [76]) and Sensata Technologies (e.g., QCM-D SPR system) [77,78], provides label-free detection and high sensitivity [79] but it suffers from interference effects. Optical sensing techniques, CEAS and PAS, available from LumaSense Technologies (e.g., INNOVA 1412i [80]) and ABB (e.g., ACF-NT™ [81]), offer high sensitivity and compatibility with remote sensing configurations. For example, CEAS relies on the accurate management of optical cavities and may necessitate advanced equipment, which restricts its ability to be easily transported and used in field applications. PAS technique, although highly sensitive in detecting small amounts of gases, can be susceptible to ambient noise and background interference, which can undermine its dependability in noisy settings. In general, when comparing Raman-based gas sensor technologies to alternative optical sensing techniques such as SPR, CEAS, and PAS, Raman spectroscopy is generally preferred due to its exceptional specificity, sensitivity, durability, and versatility. The benefits of Raman-based gas sensors make them essential instruments for various gas sensing applications, including environmental monitoring, industrial process control, medical diagnostics, and homeland security. With this vast discussion of the existing techniques and instruments in use, the practical significance of Raman spectroscopy [34,82–92] becomes more prominent. Fig. 1 represents an infograph showing the trend of peer-reviewed articles published in last seven years where Raman spectroscopy is used as a methodology for gas sensing applications. Publications were identified using suitable search terms in Scopus, such as “gas Raman”, “atmospheric Raman”, before omitting review papers, and articles pertaining to the development of materials used for gas sensing, characterised using Raman spectroscopy. The consistent pattern of studies reported in this field necessitates a compilation of knowledge for future research in this area. The technique bears a huge scope as an alternative gas sensing method where almost all gas species can be detected, and mixtures of gases can also be detected simultaneously using a single-wavelength laser. The analyte species do not require any complicated preparation, such as the removal of water, which results in a large reduction in both time and cost. This is in comparison to the few procedures that were discussed earlier. For example, SERS, available through platforms like Renishaw (e.g., inVia™ Raman microscope [93]) and B&W Tek (e.g., NanoRam® [94]), enhances Raman signals, enabling the detection of trace levels of gases with excellent selectivity. However, it may require sophisticated nanostructures and precise experimental conditions. Furthermore, Raman spectroscopy-based gas sensors signals remain unaffected in extreme temperatures and pressures.

3. Fundamental understanding

When light interacts with a molecule, the oscillating electromagnetic field of the incident photon induces polarization in the molecular electron cloud. This interaction can be described as the formation of a transient, non-quantised virtual state, where the photon is momentarily coupled with the molecule. The energy dynamics of this process vary depending on the type of scattering involved. In elastic (Rayleigh) scattering, there is no net energy transfer between the photon and the molecule. As a result, the scattered photon retains the same energy, and hence the same wavelength, as the incident photon. This type of scattering is the predominant process during light-matter interactions [95]. A small fraction of incident light is scattered in all directions when a monochromatic light beam passes through a material. An electric field can polarise or distort the electron cloud of a molecule. If one adds an oscillating electric field to the molecules (the electric vector of a light wave), the deformation of the electron cloud will oscillate with the frequency ω of the incident light beam. The oscillation of the electron cloud generates an oscillating dipole that emits at the same frequency as the incident beam. Rayleigh scattering is the name given to this mechanism. As previously indicated, it can be thought of as elastic scattering of a photon by a molecule. Rayleigh scattering can be seen in all directions. However, a close examination of the scattered radiation reveals that it occasionally contains radiation of multiple frequencies. As previously stated, Raman discovered this behaviour in 1928 and named it Raman scattering [15,95]. Raman scattering, an inelastic scattering mechanism with an energy transfer between the molecule and dispersed photon, occurs about 1 in 10 million photons. There is always a modest but finite chance that incident radiation will transfer some of its energy to the molecules' vibrational or rotational modes. If the molecule receives energy from the photon during scattering (stimulated to a higher vibrational level), the scattered photon loses energy and its wavelength rises, a phenomenon known as Stokes Raman scattering. If the molecule loses energy by relaxing to a lower vibrational level, the scattered photon gains energy and its wavelength decreases, a process known as anti-Stokes Raman scattering. While quantum mechanics allows for both Stokes and anti-Stokes scattering processes, they are not equally probable in practice. The population of molecules in various vibrational energy states follows the Boltzmann distribution [96], stating that, at thermal equilibrium, most molecules occupy the ground vibrational state. As a result, Stokes scattering is statistically more likely to occur, leading to a higher intensity compared to anti-Stokes scattering [97]. Additionally, factors such as pre-resonance Raman effects and temperature-dependent population distributions further influence the

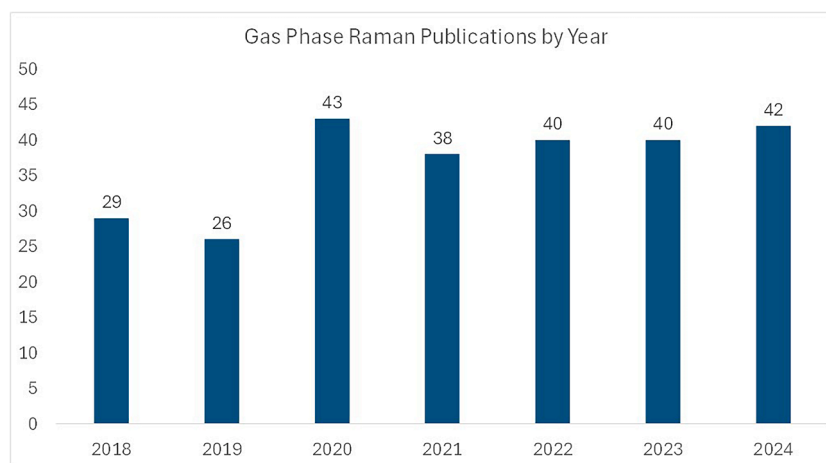


Fig. 1. Representation of peer-reviewed publication in the field of gas sensing using Raman spectroscopic techniques (in the last seven years) where Spontaneous (SRS), Stimulated (StRS), Coherent Anti-Stokes (CARS), Surface-Enhanced (SERS) and Fiber-Enhanced/Wave-Guided Raman Spectroscopy (FERS/WGRS) are included.

relative intensities of Stokes and anti-Stokes signals [98], making the situation more complex than a simple quantum mechanical equivalence. Stokes lines are of greater intensity than the anti-Stokes lines. However, these two Raman lines are extremely weak compared to the intensity of Rayleigh scattered light. Raman intensity is significantly weaker than that of the incident light. Fig. 2(a) showing scattering in Raman Spectroscopy illustrates different types of light scattering when a laser interacts with a molecule, in this case, H₂O. Incident light from the laser λ_{laser} can result in Rayleigh scattering (Elastic scattering where the scattered light has the same wavelength; $\lambda_{\text{scatter}} = \lambda_{\text{laser}}$), Stokes Raman scattering (Inelastic scattering where the scattered light has lower energy corresponding to molecular vibrations; $\lambda_{\text{scatter}} > \lambda_{\text{laser}}$) and Anti-Stokes Raman scattering (Inelastic scattering where the scattered light has higher energy (shorter wavelength, due to molecules starting in an excited vibrational state; $\lambda_{\text{scatter}} < \lambda_{\text{laser}}$). The energy level diagram in Fig. 2(b) highlights energy transitions in the Raman process. Molecules initially in the ground vibrational state (S_0) can absorb laser energy and scatter either elastically (Rayleigh scattering, where no energy is lost) or inelastically (Raman scattering). Stokes scattering involves an energy loss (transition to a higher vibrational level), while Anti-Stokes involves energy gain (transition from an excited state to the ground state). Virtual energy levels are introduced to represent the temporary energy state during light-molecule interaction. Fig. 2(c) showing molecular vibrations including Symmetric stretch (Atoms move symmetrically along the bond axis), Asymmetric stretch (Atoms move in opposite directions but not symmetrically) and Bending modes (Atoms move in a plane perpendicular to the bond, either in or out of the plane). Fig. 2(d) illustrates vibrational behaviour in a diatomic molecule (e.g., XY, XX) based on their equilibrium (The molecule is at its rest position with no

vibration) and vibrational states of being stretched (The molecule is elongated as the bond length increases) and contracted (The bond length decreases as the molecule vibrates inward). This change in ease with which the electron cloud of a molecule can be distorted (i.e., change in polarisability) is responsible for Raman activity. A detailed analysis of the classical theory and quantum mechanical principles governing these vibrational modes and scattering processes is presented in the Appendix section, where harmonic oscillators, selection rules, and quantum state transitions are discussed for better interpretation of the observed Raman shifts.

4. Types of signal acquisition

Since Raman scattering was first discovered, spontaneous Raman spectroscopy has evolved as a tool for the identification of molecular fingerprint [91]. Raman spectroscopy enables the remote detection, identification, and chemical structural study of many materials by probing vibrational and rotational molecule oscillations. In the case of sensing applications, various reports have been published touting the potential of Raman spectroscopy as both a qualitative and quantitative instrument [99–101]. The disadvantage of spontaneous Raman is the low efficiency that relates to it. In most cases, only a small portion of the scattered photons carry information about the vibrational modes of the analyte, hence this is a significant limitation of the technique. To obtain a signal-to-noise ratio that is acceptable, it is necessary to increase the amount of incident light and to use acquisition durations that are significantly longer. Due to these factors, the application of this method is restricted when it comes to investigating low concentrations of analyte and monitoring any

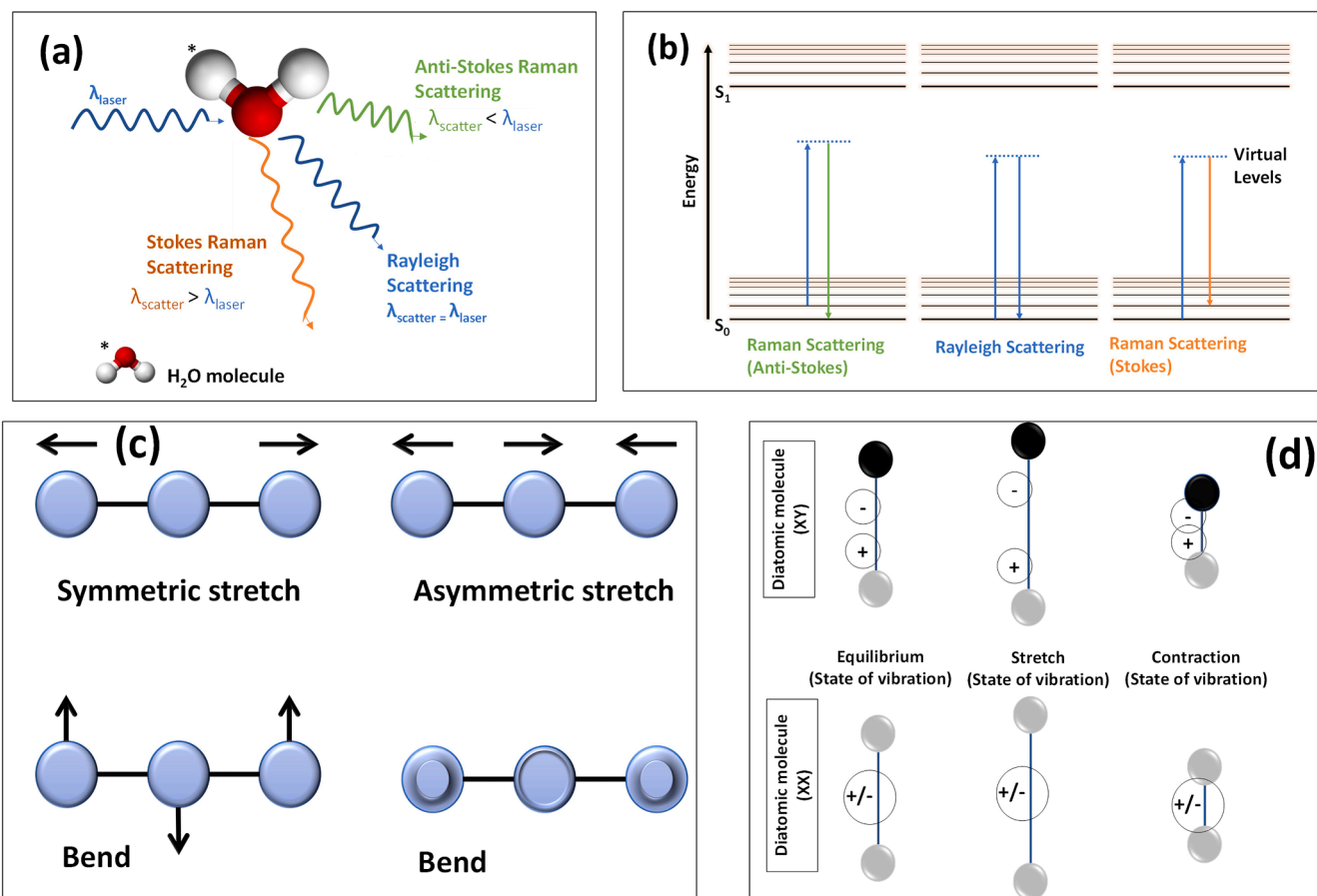


Fig. 2. Fundamental Concepts of Raman Spectroscopy and Molecular Vibrations (a) Pictorial representation of Raman scattering [226], (b) Energy Level Diagram for Raman and Rayleigh Scattering [95], (c) Depicted here are different types of molecular vibrational modes, fundamental to understanding Raman spectroscopy, (d) Change in dipole moment during different state of vibration of in case of diatomic XY and XX.

systems that are subject to rapid change (this topic is elaborated more in section 5.1). The percentage of change in polarisability of target molecules, which is equal to [102], is the selection rule for molecules to be Raman active. In accordance with the traditional conception of Raman spectroscopy, in addition to these previously mentioned parameters, the Raman intensity is also determined by instrumental (for example, the detector and the length of glass fibre when it is being used as a probe) and analyte parameters (for example, the sampling volume, the sample particle size, the refractive index of sample, and its concentration). This is done in addition to the parameters that were mentioned above. In the case of probe-based approaches, which are mostly used for gas sensors, when probes are incorporated into a process stream, the only light that is detected as a signal is light that is scattered into the same direction as where the incoming light came from. This is because this light is reflected back towards the source of the incident light. Utilising the phenomena of resonant, coherent, and surface enhancements of Raman scattering, this disadvantage can be surmounted. These effects increase the efficiency of Raman scattering, and represent distinct spectroscopic techniques: coherent anti-Stokes Raman scattering (CARS) spectroscopy, surface-enhanced Raman scattering, and surface-enhanced CARS spectroscopies (SERS and SECARS). In addition to producing stronger signals than spontaneous Raman spectroscopy, these techniques provide complementary spectroscopic data to the vibrational-rotational spectrum. They provide additional methods for investigating, among other phenomena, the electronic molecular structure, the evolution of chemical reactions, and the imaging of dynamic systems such as gas flows. The advantages of CARS over spontaneous Raman scattering spectroscopy is discussed in this review. In addition to this, StRS and TERS have further expanded the scope of Raman signal acquisition, offering unique advantages for sensitive detection and high-resolution analysis. StRS enhances Raman signals by employing two synchronised laser beams to stimulate coherent vibrations within the analyte. This leads to a significant amplification of the Raman signal with minimal background noise, making it particularly effective for real-time monitoring of fast dynamic processes. TERS, on the other hand, combines the spatial precision of scanning probe microscopy with the signal enhancement of localised surface plasmon resonance at the tip of a metallic probe. The distinct signal acquisition strategies ranging from surface enhancement in SERS, coherent amplification in CARS and StRS, to nanoscale localisation in TERS open new avenues for advanced gas sensing applications. Beside the fundamental insights of each technique, this article also includes their scope of application (section 6).

5. Fundamental principles of advanced Raman spectroscopy techniques

5.1. Spontaneous Raman scattering (SRS)

From the quantum mechanical description of the Raman spectroscopy (discussed in Appendix; 11.1), it is an accepted fact that the rotational-vibrational energy states of the molecules resemble to discrete quanta (with distinctive J values) and the energy level diagram represents the Raman processes with Stokes and anti-Stokes emission [102]. In case of physical conceptualisation of Spontaneous Raman Scattering process, the incident pump photon necessitates the perturbation of the intermediate states which commonly do not correspond to electronic states of the system and are the virtual energy states. As the frequency of the pump photon approaches the energy of the electronic states, the potency of the Raman effect improves due to resonance effects and is characterised pre-resonance Raman. If the intermediate state agrees to a discrete electronic energy state, the interaction is depicted as resonance Raman scattering and the signal strength is expected to exceed that of virtual-intermediate-state Raman scattering by orders of

magnitude. When the energy of the incident photon is in the range of dissociative energy levels, the phenomenon is termed as continuum resonance Raman scattering [103,104]. A pictorial representation is added in Fig. 3(a). As discussed in the Appendix, Raman scattering transitions between certain quantum states are not allowed and they follow a certain selection rule. The energy transitions can be either Raman active or optically active (considering the polarizability effect). In case of linear molecules, the symmetric stretching modes of vibration or bending are Raman active and are optically inactive while those with anti-symmetric modes are Raman inactive and optically active (i.e., mutually exclusive) [104]. It is a general rule for nonlinear molecules, mutual exclusion is relaxed in case of SRS. For molecules bearing no inversion symmetry, rotational-vibrational mode transition can be both Raman and optically active. In SRS, the higher intensity of Stokes than the anti-Stokes signal is corroborated to the population of energy states, governed by thermal statistics [104,105]. For bosonic systems [106], the probability of the scattering target occupying a given vibrational quantum energy state obeys Bose-Einstein statistics. For non-resonant Raman scattering and thermal equilibrium, the ratio of the anti-Stokes and Stokes scattered intensity is given by [107]:

$$\frac{I_{AS}}{I_S} = \left(\frac{\omega_p + \omega_{osc}}{\omega_p - \omega_{osc}} \right)^4 e^{\left(\frac{\hbar\omega_{osc}}{kT} \right)} \quad (1)$$

Where I_S and I_{AS} are the intensity of the Stokes and anti-Stokes light, respectively, \hbar is Planck's constant divided by 2π , k is the Boltzmann constant and T is the temperature of scattering species. However, this equation becomes erroneous for resonance Raman scattering due to occurrence of Stokes and anti-Stokes processes at different siphon photon frequencies [107]. In the case of SRS, the Raman effect is very feeble; on average, 1 in 10 [8] of the incident radiation, endures SRS [108]. It is an incoherent process as the corresponding transition from any virtual excited state to the final state may take place at any point time independently and can reach up to final state based on probability. In this case, the power or intensity of the output signal, which is the scattered light, is proportional to the input power while also being dependent on the direction of the polarisation of the molecules. The scattered spectrum generates peaks at all of the Raman active modes; the relative intensity of the spectral peaks is governed by the scattering cross-section of each characteristic Raman mode [105].

5.2. Stimulated Raman scattering (StRS)

Unlike SRS, StRS is a coherent process which includes the consideration of mixing of four- nonlinear optical wave. The modes of oscillation remains in phase to form a coherent adjustment of polarisation in the sample with susceptibility χ [$3(\omega_S; \omega_p + \omega_S - \omega_p)$] [109]. Additionally, the scattered light also stays coherent [110]. Here, $\chi(3)$ represents the third-order nonlinear susceptibility of the material. This parameter characterises the material's response to the electric field in nonlinear optical processes, such as third-harmonic generation, four-wave mixing, or Kerr effect. Essentially, it quantifies how the polarization of the medium changes with the intensity of the applied electromagnetic field. ' ω ' represents the angular frequency of the electromagnetic waves involved. In order for the StRS to function properly, the cross-section of the SRS, the path length of the light-field-matter interaction, the spectral linewidth, the input intensity, and the optical feedback (light production) of Stokes frequency light all need to be accurate [109]. When photons of frequency ω_p and ω_S simultaneously interact with a molecule staying in the ground state, the system generates vibrations with an induced frequency (ω_{osc}) and expressed as, $\omega_{osc} = \omega_p - \omega_S$. In contrast to SRS, the stimulation effect determines both the de-excitation/relaxation period and the energy level of the end state. The molecule then scatters a new photon with frequency and phase similar to that of the incident light of frequency (ω_S) as a result of the energy being transferred from the thrust photon to the molecule as a

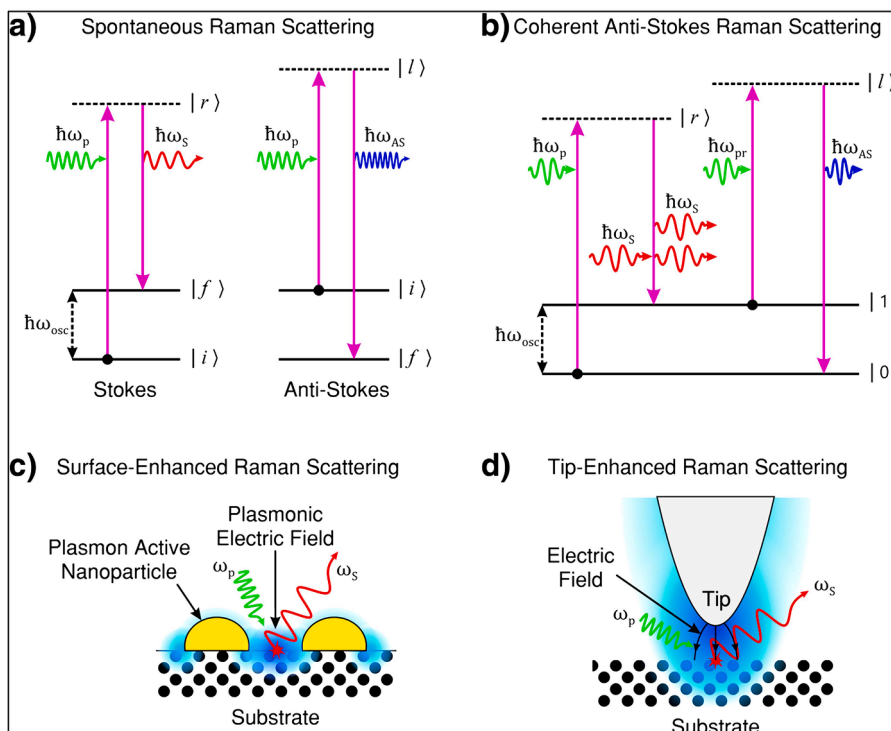


Fig. 3. (a) Energy transfer process in Stokes (left) and anti-Stokes (right) Raman scattering, in both scattering processes, the lifetime of the excited state is probabilistic and spontaneous. In Stokes Raman scattering, the initial (ro-)vibrational energy $|i\rangle$ of the scattering material is less than that of the final state $|f\rangle$, the scattered light has less energy than the pump light. In anti-Stokes scattering, the initial (ro-)vibrational energy $|i\rangle$ of the scattering medium is greater than that of the final state $|f\rangle$, the scattered light has more energy than the pump light. (b) Coherent anti-Stokes Raman scattering (CARS). CARS is a four-wave mixing process of pump, Stokes, probe and anti-Stokes light in which the emission of anti-Stokes light is coherently induced through an intermediate (ro-)vibrational energy state population inversion. (c) Surface-enhanced Raman scattering (SERS). The incident pump light induces a surface plasmon resonance. The resultant enhancement of the oscillatory electro-magnetic (EM) field strength (shown in blue) on the surface intensifies the light-matter interaction and consequently increases the intensity of the Raman scattered light. (d) Tip-enhanced Raman scattering (TERS). The incident pump light induces a tip-surface plasmon resonance associated with the plasmonically active tip. The resultant enhancement of the oscillatory EM field strength (shown in blue) is localised to the vicinity of the tip apex. The lighting rod effect (illustrated by curved black arrows) intensifies the light-matter interaction in the tip region and provides high-resolution (beyond the diffraction limit of light) Raman imaging.²⁶² [Reprinted with permission]

result of this stimulation.

An external radiation source is tuned to the Stokes frequency with the photon pump laser beam to provoke this phenomenon. Reportedly,

this technique has led to exponential gain in the Stokes signal intensity, by transferring energy from the laser radiation, and rapid population of the final rotational-vibrational state [111]. Nevertheless, when the

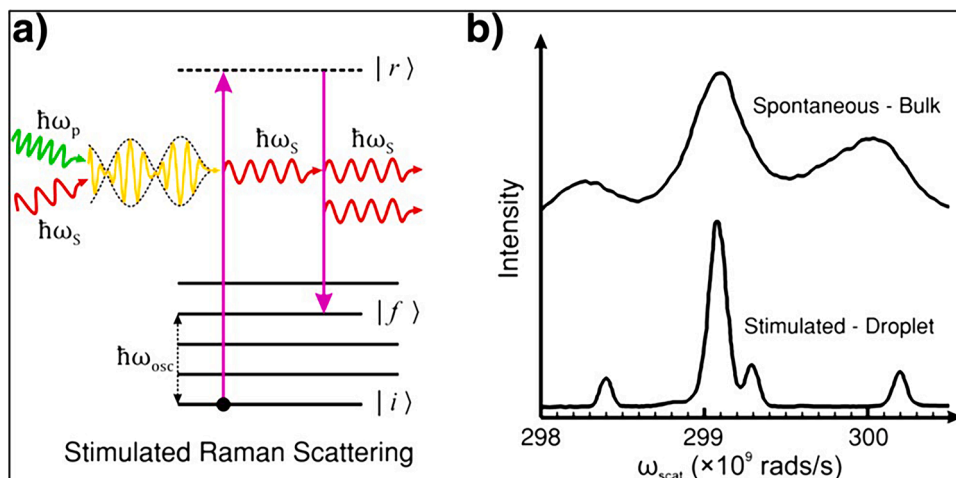


Fig. 4. (a) Energy level diagram of stimulated Raman scattering (StRS). StRS is the induced emission of Stokes light by the coherent interaction of the pump and Stokes light with the material. Unlike spontaneous Raman scattering (SRC) where the lifetime of the state and the energy of the final state are probabilistic, in StRS, the (ro-)vibration of the molecule or lattice is coherently driven by the difference frequency of the pump and Stokes light. (b) Comparison of SRC and StRS of bulk and droplet ethanol. The spontaneous measurements were performed in a cuvette (bulk ethanol). The StRS measurements were performed in a droplet of ethanol which acted as an optical resonator for the Stokes light [109] [Reprinted with permission].

intensity of the incident light of frequency ω_p is adequate, the Stokes frequency within the molecule can undergo self-promotion of StRS without any external ω_S source. However, the StRS threshold gets substantially reduced when the interaction of laser photons/pump and Stokes field gets extended in presence of an optical resonator, (e.g., internal reflection in a droplet of liquid). Fig. 4b accounts for the similar effect where the StRS spectrum is recorded with droplets of ethanol directly compared to the SRC of bulk ethanol. As predicted, the droplets act to confine the light by internal reflection which feeds back the Stokes light as a self-StRS inducing optical resonator [112].

5.3. Coherent anti-Stokes Raman scattering (CARS)

CARS is a third-order nonlinear four-wave optical mixing process. Fig. 3b shows the energy level diagram. In the CARS technique, the pump and probe laser beams (ω_p and ω_{pr} , respectively) are combined with the Stokes beam (ω_s). A tunable Stokes beam is often used to ensure that the frequency difference between the probe and Stokes beams matches the rotational or vibrational frequency of interest [113]. Finally, the probe beam causes perturbation of anti-Stokes scattering process to take place at $\omega_{AS} = \omega_p - \omega_s + \omega_{pr}$ (2). [114] A generalised expression for dominant terms in resonant CARS is given by the following [115,116]:

$$\chi^{(3)} = \frac{A_R}{\omega_{osc} - (\omega_p - \omega_s) - i\Gamma_R} + \chi_{NR}^{(3)} \quad (3)$$

Here, ' Γ_R ' is the half width at half maximum for the Raman line [115]; ' A_R ' is a constant representing the Raman scattering cross-section. The first term represents the contribution due to CARS vibrational resonance as in Fig. 3b ($\omega_{osc} = \omega_p - \omega_s$). The second term is the non-resonant background signal and is independent of the Raman shift ($\omega_{osc} \neq \omega_p - \omega_s$). Because not all quantum routes of the scattering process involve a resonance with a rotational-vibrational state, the non-resonant background develops [117]. The resonant portion of the signal is interfered with by this non-resonant contribution, and the non-resonant background results in unique distortions of the CARS spectrum compared to the SRC [118,119]. Due to this occurrence, CARS is no longer a popular technique.

5.4. Surface-enhanced Raman scattering (SERS)

The inherent weakness of signal limitation restricts its straightforward approach and thus different methods are proposed to increase the signal output, such as increase in intensity of incident laser beam, focusing strategies into microscope and which sometimes it results photobleaching of the sample [120]. SERS, a vibrational spectroscopy-based technique, can be used to identify molecules down to their fingerprint. The surface enhanced Raman signal (SERS), first noticed by Fleischmann et al. in 1974 while studying pyridine on the rough surface of a silver electrode [121], expands the range of surface enhanced Raman signal and its associated sensitivity makes it a flourishing spectroscopic method to study electron transfer reactions that could be enhanced. Regarding the conventional theory of Raman spectroscopy, it is generally acknowledged that electromagnetic and chemical mechanisms both contribute to SERS. As a result of the previous section's thorough discussion of molecular polarizability, excitation, and scattering processes, it is now clear that molecules exposed to an oscillating incident electric field undergo induced polarisation (P_0) and emit scattered light with a Raman-shifted frequency (ω_R) [122,123]. P_0 depends on the Raman polarizability of the electrons in the molecule (α_{R0}) and the strength of the incoming electromagnetic radiation E_0 (with a frequency of ω_0), as follows:

$$P_0 = (\omega_R)^{1/4} \alpha_{R0} (\omega_0, \omega_R) E_0(\omega_0) \quad (4)$$

Qualitatively, α_{R0} represents the change in the electron cloud during

the molecular vibration, and the Raman scattering involves the interaction between two basic aspects, a molecule and an incoming radiation. SERS involves the interaction among light, molecule, and metallic nanostructure. Metal nanostructure being irradiated with an incoming light (E_0), the conductive electrons get delocalized into collective oscillations, generating an electromagnetic field around the interface formed by the metal nanostructure and the dielectric environment (Fig 3c). The frequency of such electron oscillations depends on the density of electrons, the effective electron mass, and the shape and size of the charge distribution. If the frequency of the radiation (ω_0) is in resonance with that of the electronic oscillation, the corresponding excitation process is stated as surface plasmon resonance (SPR). Similarly, other causes of oscillation, such as dipoles (P_0) or quadrupoles lead to the excitation of the localised surface plasmon resonance. The Raman polarizability of molecules interacting with metal nanostructures (P_0) in the case of SERS often results in values that are one to three orders of magnitude higher than those of the molecules' free states. Thus, the mutual activation of the Raman polarizability by the local EM field results from the interaction of molecules with the nearby metal nanostructures, and vice versa. For low vibrational Raman modes frequency, ω_0 can be considered roughly equal to ω_R , and the electromagnetic enhancement factors $G_{ex}(\omega_0)$ and $G_R(\omega_R)$ becomes comparable. Hence, the overall enhancement of the electro magnetic field in SERS (G) can be represented as:

$$G = \frac{|E_{Loc}(\omega_R)|^4}{|E_0(\omega_0)|^4} \quad (5)$$

Further study of this technique has been avoided since it would entail material/substrate specific enhancement factors of SERS, which is outside the purview of this review. Considering the topic of the article, which is limited to the use of Raman spectroscopic techniques only for gas sensing applications, this article has refrained from discussing this technique further. Nevertheless, the reports and works involving SERS for gas sensing or the construction of sensing equipment are presented in section 6.4 in a comprehensive and extensive manner.

5.5. Tip-enhanced Raman scattering (TERS)

An advancement on the SERS method, tip-enhanced Raman Scattering also relies on inducing an electromagnetic field through the sample material to increase the overall signal strength and resulting spectral intensity. Where TERS differs from SERS is in its spatial resolution capability. The signals from a SERS measurement are not site specific but are from the total area irradiated by the Raman laser, as with most conventional Raman spectroscopic methods (Fig 3d). Optical imaging instruments are typically diffraction-limited systems, in that their resolvable distance is a function of the wavelength of the probe photon and the numerical aperture of the instrumentation; $d = \lambda/2NA$ (6) [124]. In TERS, the sharply etched metal tip is used to localise the electromagnetic field enhancement described for SERS in section 5.4 to a much finer, and spatially resolved location on a sample surface. The tip and laser focal point can be moved over the sample surface, and maps generated of the surface of a material [125], or the tip may remain stationary to observe dynamic processes such as catalysis reactions [126]. For the same rationale as provided in section 5.4, further discussion on TERS will be refrained from, and further works on the application of TERS will be presented in section 6.5.

6. Recent advances

6.1. Detection using SRS

Raman spectroscopy is one of the most studied spectroscopic methods. This approach can identify individual gases in a mixture in real-time. While portable devices are also being developed for medical

or environmental fields, such as breath analysis or pollution management, a considerable number of researchers have taken advantage of this technology for gas sensing. The common gaseous species that are currently being monitored are listed in Table 1 along with their related Raman shifts and cross sections. Raman scattering is dependent on the scattering cross section area of the involved molecule, which is relatively low for gas molecules. For example, if N_2 at room temperature and pressure (contained in a transparent cell) is focused with a laser source of 785 nm, ≈ 100 mW (free-space setup), a Raman Stokes power output of $\approx 10^{-14}$ W is obtained since the scattering cross section of N_2 at 785 nm is equal to 7.467×10^{-32} cm²/sr•molecules [127]. An important factor in the free-space experiment is the interaction length between the gas molecule and the laser beam, which is almost twice of the Rayleigh length of the focused beam [128]. Distributed temperature sensors (DTS) exploiting SRS effect is widely utilised in gas and oil industries for remote temperature monitoring and detection of leaks in oil wells. These systems are often required to withstand extended exposure to harsh environmental conditions and high temperatures. The temperature can reach up to 380°C in geothermal wells [129]. Buric and his group coined the solution to increase the interaction length of Raman signal by introducing hollow core photonic crystal fibres (HC-PCFs) [130]. The periodic cladding structure of these type of fibres makes it a good wave guide in the lower refractive index hollow core. When analyte gas is purged/passed through the guided core of a HC-PCF, it provides longer interaction lengths between the incident laser and the gas molecules. With this setup, a hundred times of enhanced intensity of Raman signal (Stokes lines) could be obtained than that of in free-space [130,131].

As discussed previously, the intensity of the Raman signal is proportional to the differential scattering cross section of the molecule and it can a function can be deployed that computes the intrinsic rate at which the scattered photons can be detected at a given angle,

$$\frac{\delta\sigma}{\delta\Omega}(\omega_s) = \frac{1}{9} \frac{(\omega_1 \omega_s^3)}{(\pi^2 \epsilon_0^2 \hbar^2 c^4)} \text{Im}\{R(\omega_s, \omega_s - \omega_1, -\omega_1)\} \frac{m^2}{sr} \quad (7)$$

where:

- ω_s = frequency of the Raman scattered light.
- $\Delta\omega$ = Raman Shift, this is the difference between the frequency of the exciting light and ω_s .
- $\omega_1 = \omega_s + \Delta\omega$ = Laser frequency.
- R represents the transition rate between the two states $|i\rangle$ (initial state of the molecule) and $|n\rangle$ (excited vibrational or rotational state of the molecule).

The above equation also shows the dependency of differential scattering cross section on the frequency of the laser source.

Since the Raman shift is representative of the vibrational (or rotational) properties of a molecule, it is possible to extract a molecular fingerprint from a molecule that is Raman active. This was covered in the previous section. In this waveguided apparatus, one may get a straightforward formula for the strength of the Raman signals as:

$$I_s = k I_L \rho (\partial\sigma / \partial\Omega) \Omega \quad (8)$$

where, ρ is the molecular number density in the measurement volume V in molecules / cm³, Ω is solid angle observed, L is the length of the measurement volume / interaction length between the beam and the sample. I_L is the intensity of the light hitting the molecule and k is the setup constant depending on geometry and wavelength-dependent losses. The linear dependence from L, leads to the advantage of using hollow core fibres as the entire length of the fibre represents the interaction length between the gas contained in the hollow core, and the laser beam. Buric and his group experimented by sending the light from a 514.5nm laser into 1.5m long section of commercial PBGF containing N_2 at ambient pressure and they also used the same laser for the free

space detection of output with a photomultiplier. In the next year, by using a different set-up arrangement, Buric and al. [131] further improvised back-scattering configuration, in which both the laser input and Stokes output (backward wave) occur at the same end of the fibre. The report of Afsar et al is also in agreement with the enhanced output in backscattering set up for SRS [148]. As an added advantage, detection of low-pressure gases in the ≈ 100 ppm range could also be achieved using the new setup while Chen and his group detected rotational lines of nitrogen and oxygen for the first time by using a 1 m length of waveguide [149] in a back-forward setup configuration. SRS enables one of the gifted applications of Raman gas sensing in the field of breath analysis. Reportedly, the presence of certain gases in an exhaled breath can be treated as a biomarker for some disease as lung cancer, diabetes [150] and many more and SRC serves as a useful technique here. Hanf et al. [135] used PBGF in a SRS based fibre-enhanced (backscattering) Raman spectroscopy (FERS) setup to detect the contents of a mixture of climate relevant gases and a human breath sample (Fig. 5) and could accomplish a sensitivity of 0.2 ppm for CH_4 and a dynamic range of about four orders of magnitude using 2 W of a 532.2 nm laser and 20 bar of pressure. The results highlighted the high potential of fibre-enhanced Raman spectroscopy with hollow-core photonic crystal fibres as minimal volume cuvettes for quantitative analysis of isotopic tracers. Additionally, Chow et al. were able to use SRS in a forward setup arrangement to acquire the rotational lines of pure O_2 and pure H_2 at 14 bar and 7 bar, respectively. The CO_2 [151] Raman bands were obtained by Chow and his team. The publications that have already been published on SRC-based gas sensing also make an intriguing association between the source's wavelength and its associated sensitivity during the procedure. Although it is outside the focus of this paper, it is important to consider this fundamental issue when comparing the outcomes of experiments using various SRS setups, analytes, sources, etc. It is important to note that operating pressure and waveguide length both play a role in obtaining the Raman signal during the SRS process [25]. Lambrecht, and his team reported detection of CO_2 in ambient air at one bar, proving a sensitivity of ≈ 380 ppm using 20 mW laser power (785 nm laser) and an integration time of 100s [152]. Evidently, the SRS technique appears to be extremely dependent on the addition of various types of OF in order to improve or adjust the range of integration time, detection limit, and sensitivity, among other things [153]. Concluding the section with the recent article of Brooks et al. [154] reporting on the development of a compact gas-phase Raman based instrument (Fig. 6a) using a hollow core anti-resonant tubular fibre where they have proposed a commercially viable Raman prototype instrument exploiting a tubular hollow-core anti-resonant fibre-based approach [155] by primarily increasing the optical interaction path (also fulfilling the gas sampling component of the instrument). They successfully reported the detection of O_2 , N_2 and H_2O (g) from ambient atmospheric samples (Fig. 6b-c) and commercially supplied CO_2 , CH_4 and C_3H_8 at ambient temperature (Fig. 6d). Recently Bai et al. [156] and his group integrated Hollow-core anti-resonant fibres (HC-ARFs) into the Raman system to explore practical detection limits in the field of gas sensors. The limits of detection (LODs) of their developed system have 1.2 ppm bar for CH_4 , 2.9 ppm.bar for C_2H_6 , 1.6 ppm.bar for C_2H_4 , 2.7 ppm.bar for C_2H_2 , 13.8 ppm.bar for H_2 , and 16.7 ppm.bar for CO when an excitation laser of 200 mW was used with an exposure time of 60s. This improved level of detection has pushed the technology one step ahead in terms of practical applications.

6.2. Detection using StRS - stimulated Raman scattering

The StRS technique uses two spatially and temporally synchronised laser beams (pump and Stokes beams) to coherently excite molecular vibrations [157]. When the frequency difference between the two pulsed lasers matches that of a molecular vibration, quantum stimulation of

Table 1

Raman shifts for common pollutants and target analytes. Abbreviations: Weak Band (WB), Strong Band (SB), Broad Band (BB), (* at 532 nm).

Categories	Analyte	Raman Shift (cm ⁻¹)	Interferences	Cross Section of major peak (cm ² /sr)	References	
Combustion Gases	CO ₂	1285, 1388 (SB)	SO ₂	35.6 × 10 ⁻³²	Kiefer. J et al. [132]	
	CO	2143		9.1 × 10 ⁻³²	Kiefer. J et al. [132]	
	H ₂ O	1640, 3000-3700 (BB)	CO ₂	High	White. S et al. [133]	
	NO ₂	1316		Low	McCole Dlugosz. E et al. [134]	
	NO	1875		5.5 × 10 ⁻³²	McCole Dlugosz. E et al. [134]	
	N ₂ O	1300, 2224		2.7 × 10 ⁻³¹	Hanf. S et al. [135]	
	SO ₂	1151 (SB)		3.08 × 10 ⁻³⁰	Aggarwal. R et al. [136]	
	SO ₃	1035, 1375		CO ₂	6.7 × 10 ⁻³¹	Yanfeng. F et al. [137]
	CH ₄	1535 (WB), 2917 (SB)				Kiefer. J et al. [132]
	Volatile Organic Compounds	C ₂ H ₆		993, 2914 (SB)	CH ₄ , C ₃ H ₈	Low
C ₃ H ₈		870, 2908 (SB)	CH ₄ , C ₂ H ₆ ,	5.8 × 10 ⁻³¹	Kiefer. J et al. [132]	
			C ₄ H ₁₀			
CH ₃ Cl		725, 2874, 2965, 3043			Fedoseeva et al. and Drysdale, C et al. [145, 146]	
CH ₃ Br		609, 1304, 2819 2971, 3050			Fedoseeva et al. [138]	
CF ₄		453, 631, 908, 1283			Fedoseeva et al. and Cleis, R. A et al. [138, 139]	
CCl ₄		221, 318, 459, 756, 794			Fedoseeva et al. and Cleis, R. A et al. [138, 139]	
C ₄ H ₁₀		827, 2890 (SB)	CH ₄ , C ₂ H ₆ , C ₃ H ₈	High	Kiefer. J et al. [132]	
C ₆ H ₆ (as Benzene)		992		Low	Jochum. T et al. [140]	
Other Monitored Pollutants		Dioxins	2893, 2969	CO ₂ , O ₂	3.25 × 10 ⁻³¹	Borowski. P et al. [141]
	Furans	1139, 1485, 3158	Kim. T et al. [142]			
	PCBs	Various WBs, 1280, 1589	Cheng. J et al. [143]			
	H ₂ S	870, 2610 (SB)	Hippler. M et al. [144]			
	Cl ₂	554 (BB)	Aggarwal. R et al. [136]			
	HCl	2886	Murphy et al. [145]			
	HF	1588	Fedoseeva et al. [138, 139]			
	HBr	2560	Murphy et al. [145]			
	NH ₃	934, 967	3.68 × 10 ⁻³²			Aggarwal. R et al. [136]
	NH ₄ Cl	2141, 3045	Drysdale. C et al. [146] and Hayez. V et al. [147]			
Ambient Gases	CS ₂	658, 802			Murphy et al. [145]	
	N ₂	2331 (SB)		2.9 × 10 ⁻³¹	Kiefer. J et al. [132]	
	H ₂	587, 4156 (SB)		2.2 × 10 ⁻³¹	Kiefer. J et al. [132]	
	O ₂	1555 (SB)		1.2 × 10 ⁻³¹	Kiefer. J et al. [132]	
	O ₃	702, 1103		4.0 × 10 ⁻³¹	McCole Dlugosz. E et al. [134]	

photon in the Stokes beam amplifies the intensity of the otherwise weak spontaneous Raman scattering. As a result, the intensity of the Stokes beam is increased (SRG¹) and the intensity of the pump beam experiences a loss (SRL²). This Loss and gain are proportional to the pump power, light-sample interaction length and sample concentration [158].

The StRS systems can be broadly categorised into broadband and narrowband techniques depending on the laser system used. The combination of the narrowband and / or broadband pulses used, impacts the detection system required and the time resolution of the experiment [110]. A typical narrowband StRS system is composed of a fixed frequency laser (ω_1) and a tuneable frequency laser (ω_2) to scan across the wavelengths of interest. For narrowband StRS, a number of Stoke beams are required to build a spectrum while by using a broadband StRS an entire vibrational spectrum can be collected in one acquisition. In broadband StRS systems one or more of the lasers has a pulse width larger than 100 cm⁻¹ while all laser pulses in a narrowband StRS are < 20 cm⁻¹ [110].

It is reported that StRS can achieve a temporal resolution of 1 μ s per pixel (0.1-10 s for a spontaneous Raman microscopy) [159], a spatial resolution of 100 nm and a chemical sensitivity of 1 μ M [157]. In this technique the synergy of the pump and probe beams accelerate Raman scattering by up to x10 [8, 160]. In addition, StRS has perfect linearity with concentration of chemical bonds which means that by using this technique concentration of the target compound can be determined

[161].

The high sensitivity, fast scanning speed and fine spatial resolution of StRS make this technique extremely valuable. Recently, Chen et al. reported a summary of the most commonly reported applications of StRS [159]. The most known application of this technique is label-free imaging in biomedical applications as opposed to optical methods such as fluorescence microscopy. No specialised probes or labels are needed with StRS since the presence of chemical bonds can be confirmed using their vibrational modes alone. Fleury et al.'s work on imaging micron-sized zeolite crystals in 2018 is one of the first attempts in using polarized StRS microscopy for the field of materials science [162]. Prior to this, this technique was almost exclusively used for biomedical applications. Therefore, application of this technique in the field of materials science and specifically for gas samples is yet to meet its full potential. This developing technique carries some limitations too. For example, StRS is not suitable for samples with strong optical absorption to the pump or the Stokes beam. In addition, since this technique is mainly designed for biological samples and their vibrational bands typically fall between 1200 to 3600 cm⁻¹ wavenumbers, StRS is generally optimised for this range [157, 163]. However, modification in the optical circuit may bring Stoke and pump optical beams closer to allow detection of wavenumbers down to 300 cm⁻¹. Improvements in spatial resolutions can advance the application of this technique in the field of materials science. Currently, a near infrared light source is typically used to enable better penetration into biological samples. However, visible light can also be used to improve the spatial resolution of StRS. Ozeki et al. [164] demonstrated molecular spectral imaging of different animal tissues (including rat liver tissue and mouse intestinal

¹ Stimulated Raman Gain

² Stimulated Raman Loss

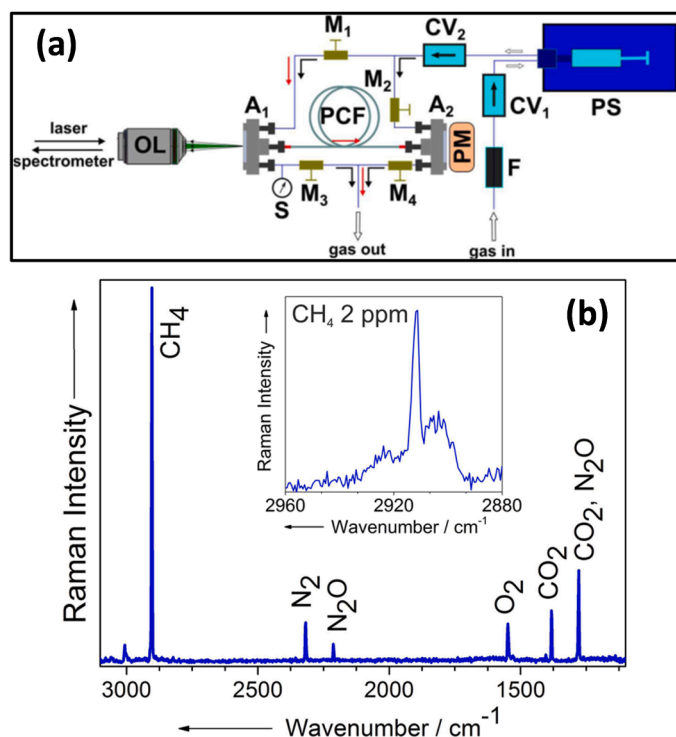


Fig. 5. SRS based setup for human breath analysis: (a) Sketch of the setup for fast and precise filling of the HC-PCF with gas mixtures consisting of mid pressure pump system (PS), fiber adapter assemblies (A1 and A2), check valves (CV), magnetic valves (M), powermeter (PM), hollow-core photonic crystal fiber (PCF), objective lens $20\times/0.5$ (OL), sensor for pressure and temperature (S), and sinter filter (F); and (b) Fiber-enhanced Raman spectrum of a biogenic multigas composition, consisting of climate relevant gases CO₂, CH₄, and N₂O together with N₂, O₂ (each ~ 1 vol %, in Raman inactive argon carrier gas), which was acquired with one single measurement within a 40 ms acquisition time. All gases are spectrally well-separated from each other and can easily be quantified simultaneously. The inset shows a separate measurement, the fiber enhanced Raman spectrum of naturally concentrated CH₄ at 2 ppm in air with SNR = 28 and thus sub-ppm LOD [135] (reprinted with permission).

villi) using high speed StRS microscopy. They reported lower Raman intensity in the fingerprint region ($500\text{--}1800\text{ cm}^{-1}$) compared to C–H stretch region ($2800\text{--}3100\text{ cm}^{-1}$). Generally, techniques such as StRS and CARS do not produce uniform signal quality across the whole Raman spectrum [165]. Bi et al. [166] reduced the femtosecond laser wavelength to the visible region and demonstrated a StRS microscope with sub-diffraction resolution down to 130 nm (from 180 nm limit) and an improved resolution ($\times 23$) due to increased photon energy. They used beta-barium borate (BBO) crystals to double the frequencies of their 1040 nm and 900 nm laser beams. In 2012 Malevich et al. [167] reported the first proof-of-principle experiments demonstrating backward coherent Raman scattering as a tool for remote chemical sensing of trace gases. They used a high-power lasing system to derive narrowband UV pulses acting as Stokes pulses and a synchronised tuneable UV pump laser, 310–350 nm, (made tuneable using a nonlinear frequency conversion system) to study responses from atmospheric gases including N₂ (at 2030 cm^{-1}), O₂ (at 1555 cm^{-1}) and methane (at 2915 cm^{-1}). They probed the gas samples with the counter-propagating narrowband Stokes pulses guided into each other using mirrors to mimic standoff detection. For remote sensing, it is necessary that the probe pulse has duration of a few nanoseconds. For atmospheric lasers (e.g., N₂ lasers) this criterion is readily fulfilled (the pulse duration can be determined by the length of filament and the lifetime of excited N₂ molecules [167]). Authors believe that the key challenge with this technique is the difficulty with detection of the Raman Gain over Raman Loss sitting on top of

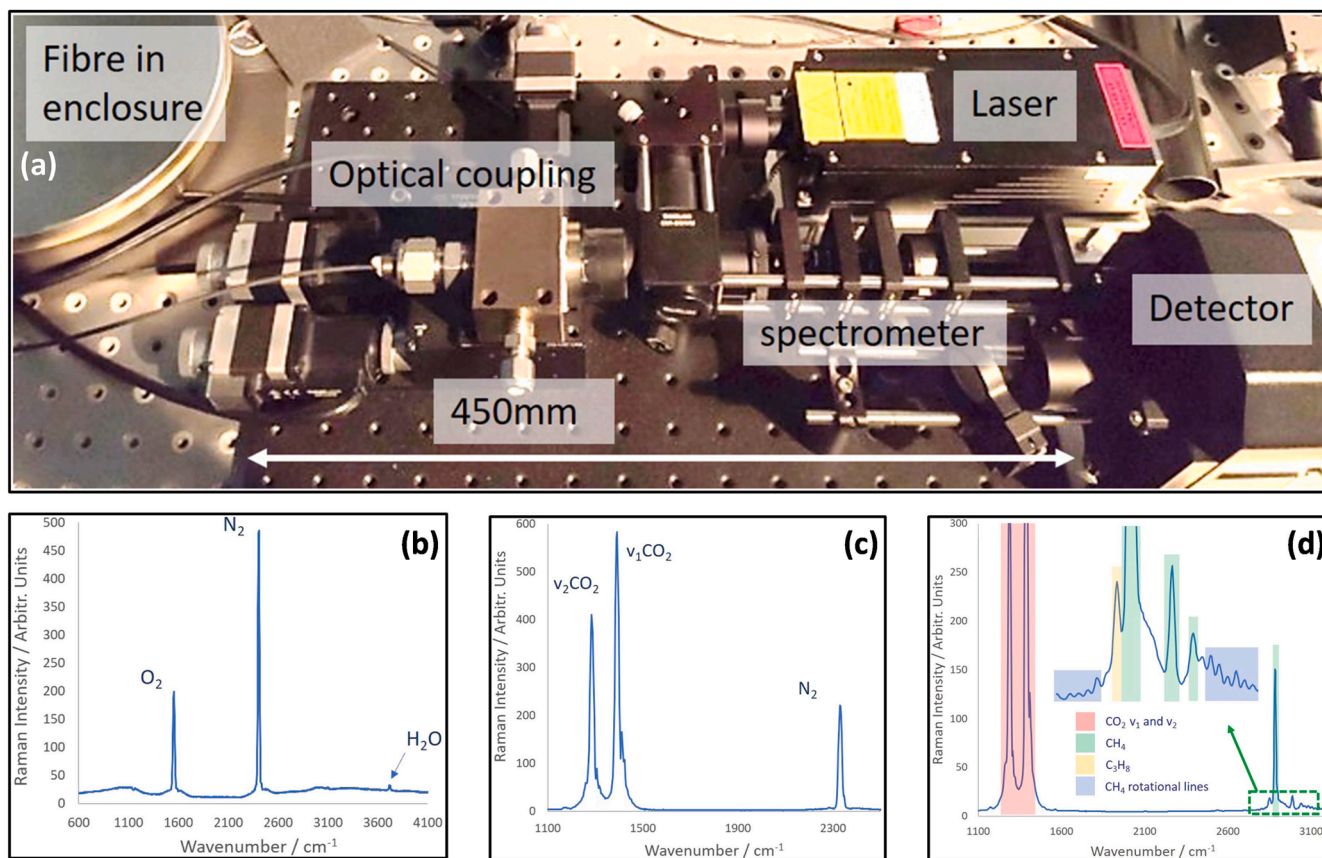
an intense noisy Stokes/pump pulse. This team defined the optimum laser parameters for remote sensing using a backward StRS setup [179]: (i) a fixed-frequency laser as the backward-propagating laser with a pulse duration in the nanosecond range and (ii) a high energy and tuneable forward-propagating laser and its pulse bandwidth should match that of typical molecular linewidth in gases. Malevich et al. [167] demonstrated the linear relationship between Raman Gain signal and the concentration of the sample. They reported detection of an SRG signal for pressures as low as 40 mbar. The SRG signal reached a value of 10^{-5} which they corresponded to the noise floor of the setup with an integration time of 1 s. The low SRG was explained by the extremely short interaction length, limited pump pulsed laser energy and the no optimum bandwidth of the pulse. They also compared the performance of a ps/ps laser system to that of a ps/ns laser system. Although the latter system presents added complexity to the synchronisation of the two lasers, it can increase the interaction length and decrease spectral width of the Stokes pulse. In 2015 Malevich et al. [168] demonstrated a remote gas sensing system using StRS in a standoff geometry (as shown in Fig. 7). In this setup a high-energy mid-IR femtosecond pulse was used to trigger atmospheric N₂ laser and provide the backward-propagating pump beam. This setup showed a detection limit of 2 bar for methane gas. Although improvements to the sensitivity of the system is necessary (for e.g., using higher energy excitation pulses), this work showed the feasibility of a backward StRS system without the need for reflection of a forward-directed excitation beam. In a more recent study Yang et al. [158] reported a H₂ gas detecting system with a hollow-core fibre that showed potential as a StRS-based gas sensing system with ppm detection level and an average response time of 250 s. In their preliminary study, the pump and Stokes laser beams were set to have a wavelength around 1532 and 1620 nm, respectively to match the S₀(0) rotational transition of parahydrogen with a Raman shift of 354.36 cm^{-1} .

6.3. Detection using CARS - coherent anti-Stokes Raman scattering

While the CARS technique was first reported by Maker and Terhune in 1965 [169], the acronym was coined in 1974 by Begley and co-workers [170]. It is believed that the first CARS-based microscope was developed in by Duncan et al. [171] in 1982. Since then and with the advancements made in the field of laser technology multiple implementations of CARS technique have been reported. Similar to StRS, CARS has been used extensively for biochemical and biomedical imaging [172,173]. This technique has been shown to be valuable for gas phase analysis [174] and catalytic reaction monitoring [175] as well. Currently, research works in this field are devoted to development of CARS instruments higher sensitivity and acquisition speed. Examples of such works are highlighted later in this section.

In the CARS technique, the pump and probe laser beams (ω_p and ω_{pr} , respectively) are combined with the Stokes beam (ω_s). A tuneable Stokes beam is often used to ensure that the frequency difference between the probe and Stokes beams matches the rotational or vibrational frequency of interest [113]. Finally, the probe beam causes perturbation of anti-Stokes scattering process to take place at $\omega_{AS} = \omega_p - \omega_s + \omega_{pr} - - (2)$ [114].

Generally, coherent Raman spectroscopy techniques are capable of generating signals 10 [5] to 10 [7] times higher than incoherent spontaneous Raman spectroscopy [114,176]. Narrowband CARS enables fast image collection but from a narrow region (3 cm^{-1}) of the Raman spectrum while broadband CARS is capable of capturing large spectral range from $\approx 500\text{ cm}^{-1}$ to 3500 cm^{-1} at longer dwell times per pixel [165]. However, due to interference of nonresonant background CARS spectrum differs from that of spontaneous Raman spectrum. This complicates spectral assignments and causes difficulty in image interpretation and limits detection sensitivity [161,174] specially for hydrocarbon-rich compounds which have higher nonresonant susceptibility [177]. In contrast, StRS provides background free chemical contact and this is its key advantage over CARS [157]. Roy et al. [174]



2021 IS-Instruments. *Journal of Raman Spectroscopy* published by John Wiley & Sons Ltd.

Fig. 6. (a) Image of the Raman instrument layout showing key sub-system components (marked within), (b-d) represent Raman spectra collected from an air sample, CO_2/N_2 sample captured at a particular time and gas mixture, containing 0.32% propane (C_3H_8), 3.68% methane (CH_4) and 96% carbon dioxide (CO_2) respectively. Reprinted from [154]

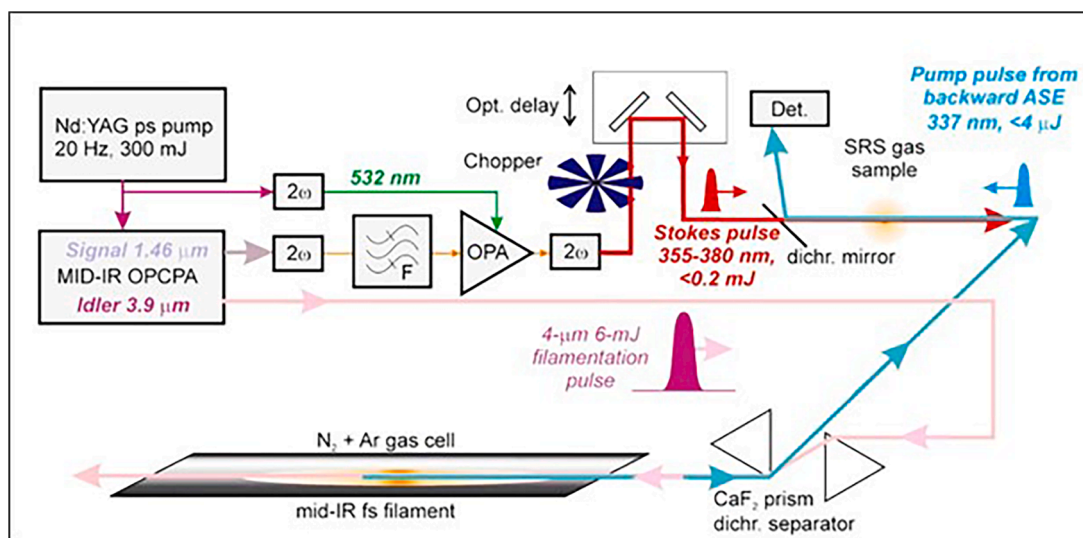


Fig. 7. The schematic illustration of the experimental setup reported by Malevich et al. In this system, two synchronized pulses (a Stokes pulse and a high-energy mid-IR pulse) are generated in forward direction. Reprinted from [168].

reviewed the advancements in the application of nanosecond to femto-second CARS in gas phase reacting flows between 1996 to 2010. According to their review, the key emphasis of the CARS developments during this period was on application of this technique to harsh chemical environments as well as application of advanced laser systems to

improve sensitivity and data acquisition speed. For example, the nonresonant background contribution in CARS can be suppressed using picosecond-CARS by temporally delaying the probe beam relevant to the pump and Stokes beams [174]. Femtosecond-CARS provides enhanced data acquisition bandwidth compared to the other two techniques in

addition to reduced non-resonant background. Sugimoto et al. [178] reported on the practical use of CARS for hydrogen leak detection (the light source setup is displayed in Fig. 8). They used a laser with short wavelength (355 nm) which is generally preferred for CARS technique. Using a beam splitter, they generated two optical paths to realise the optimal irradiation intensity ratio between the pump and Stokes beams. Briefly, they placed a 40 mm Raman cell in one of the paths to generate Stokes scattering independent of the pump light intensity. The Raman cell used was a Stokes light source filled with H₂ (0.5–0.7 MPa) capable of generating Stokes beam when irradiated with incident laser beam. The Stokes and pump beams were then irradiated simultaneously to the gas sample and the resultant anti-Stokes scattering was separated by a dichroic mirror and its intensity was measured using a spectrometer. Based on this setup, the highest anti-Stokes scattering intensity was generated when the ratio of Stokes beam intensity to that of the pump beam ranged between 0.140 and 0.173. In addition, their setup was shown to have a lower detection limit of 157 ppm well below the typical detection limit of 500 ppm for H₂ leak detection application. A great advantage of using this CARS setup for gas leak detection is its in-situ atmosphere detection capability without the need for a gas suction system. This simplifies the instrumentation design and improves detection efficiency. In 2014 Zaitso and Imasaka [176] reported a cavity-enhanced Raman spectroscopy technique based on intracavity CARS process and explored the application of this method for high sensitivity gas detection. The intensity of CARS signal is limited by the phase-mismatch³ between the laser beams regardless of the interaction length in the optical cavity in the cavity-enhanced CARS. To overcome this, authors used highly reflective mirrors with negative group delay dispersion as a cavity component and to derive the total dispersion and thus, the lasers phase mismatch to zero. Their experimental work showed that by using this method three orders of magnitude increase in the CARS intensity for H₂ gas can be detected. Although the detection limit of this setup was not evaluated in this work, the technique seems to have the potential to be used for trace gas detection. In 2013 Bohlin and Kliewer [179] reported the development of a single-shot 2D-CARS technique for collection of spectral information of gas samples in multiple spatial dimensions simultaneously. This can be of particular use in the field of combustion pollutant formation. Thus, it is safe to say that CARS technique has seen unprecedented growth since the development of the very first CARS microscopy in 1982. This technique has evolved from a laboratory-based tool to an accessible technique with applications in a wide range of fields. The key advantage of CARS is the use of anti-Stokes scattering process which eliminates limitations associated with fluorescence. Contribution of nonresonant background is a key challenge to overcome with CARS. Advances and refinements of the CARS methods thus far have reduced background contributions to CARS spectrum.

6.4. Detection using SERS

Due to its quick detection speed and excellent sensitivity, the Surface-Enhanced Raman Scattering (SERS) approach is currently being widely used to create sensors for gas detection [180–182]. Raman spectra can be used to gather fingerprint information due to the characteristic vibration frequency of molecules, as discussed in the preceding section (Section 5.4). Now that the signal from the Raman spectrum has been processed, it may be possible to successfully classify and identify samples discovered by the SERS sensor for practical field applications. A few SERS-based gas/volatile organic compound (VOC) detectors are included in this section. It is important to note that to maintain the article's one-way orientation towards the development of gas sensors solely, the advancement in the field of detection of various analyte

molecules (such as biological, chemical, etc.) is not covered here. The enhanced Raman scattering is now known to be primarily caused by electromagnetic enhancement brought on by localised surface plasmon resonance (LSPR) on the surfaces of noble metal components and nanostructures [183,184], and the chemical enhancement that results from the electronic interactions between the analyte molecule and metal species/substrate [185]. The establishment/selection of metal nanostructure is significantly essential for producing the enhanced electromagnetic field. Mostly colloid-based (solution based and less expensive) and solid surface-based substrates are commonly used SERS-active substrates [186] where the former ones are used in large-scale production and the later one (nanoparticles stabilized solid substrates) providing higher reproducibility and more stable signals for target molecule interactions [186]. To the best of our knowledge, Wong and his team first reported [187] multiplex SERS based VOCs detection with leaning nano-pillar substrate and additionally multiplex detection for the mixture of acetone and ethanol vapor could be achieved. Fig. 9 represents a schematic of the SERS based detection method. Lauridsen et al developed a SERS nanochip, optimised for detection of trace amounts of biomarker from breath and it which was mounted inside a Tedlar bag, which the patient breathed into. The SERS chip was then analysed using a Raman spectrometer and investigating the C=N peak at 2131 cm⁻¹ and correlated with sputum cultures, the detection could be made [188]. The lower limit of detection of target analyte was down to 18 ppb. Oho and his team were able to establish a quantifiable relationship between target gas adsorption/signal intensity and SERS film temperature. Finally, with the SERS film temperature of approximately 80°C, which fits with the theoretical prediction, it was possible to study the enhancement of corresponding gas adsorption and signal strength by up to 40 times. With a 2-min acquisition time, this raised the detection limit for benzene gas to 3–1 ppb. Here, they utilised Ag nanorod array sheets functionalized with propanethiol for SERS, a spectrometer equipped with a fibre Raman probe, and a 785-nm pump laser. Using this SERS-based approach, it was possible to track down the target analyte, anionic state of the adsorbate and showed it to be analogous to intramolecular Franck – Condon resonance Raman scattering [185]. There are a large number of various substrates that have been reported for the particular or targeted detection of analyte dependent on the tuneability of surface plasmon resonance (mostly). However, the full studies on substrate variability have not been included in this article because that is not the focus of the discussion here. Nevertheless, a table has been designated to show them in their individual forms. Continuing to incorporate additional SERS approaches into use, fairly recent research could be traced back to a group in Japan where Li Chen and his team offered an easy fabrication method. This paper was fascinating, and it was published just last year [189]. They claimed a wide-ranging application for constructing a SERS sensor array with different gas affinities, where the fabrication was done by spin-coating distinct functional polymer films for the identification of gases with similar structures (Fig. 10). They used functional two-layer polymer film in the sensor array, possessing a distinctive gas response, and efficiently fabricated in a simple way with high design flexibility by utilizing the layer-by-layer method. Gas detection implementation could be improved by increasing the number of characteristic variables in the response matrix processed by the e principal component analysis algorithm. This study drags the SERS technique one step ahead by experimentally proving the detection of similar type of gas analytes and thus reinforcing the credibility of this method regarding the molecular fingerprint detection in the field of gas sensor (Fig. 11). Despite the existence of numerous other reports on SERS substrates and analyte detection, this section is now intended to be concluded after highlighting the significance of SERS with regard to improving the absorbability of gaseous molecules on SERS substrate and insensitive detection of weak Raman intensities of gas molecules. There are 42 Raman active lung cancer VOC biomarkers with having concentration in the range of 10–100 ppb [190,191] and Zhang et al. [192] developed an innovative strategy for ultrasensitive detection (down to 2

³ The phase-mismatch is caused by the propagation of the interacting beams through the medium.

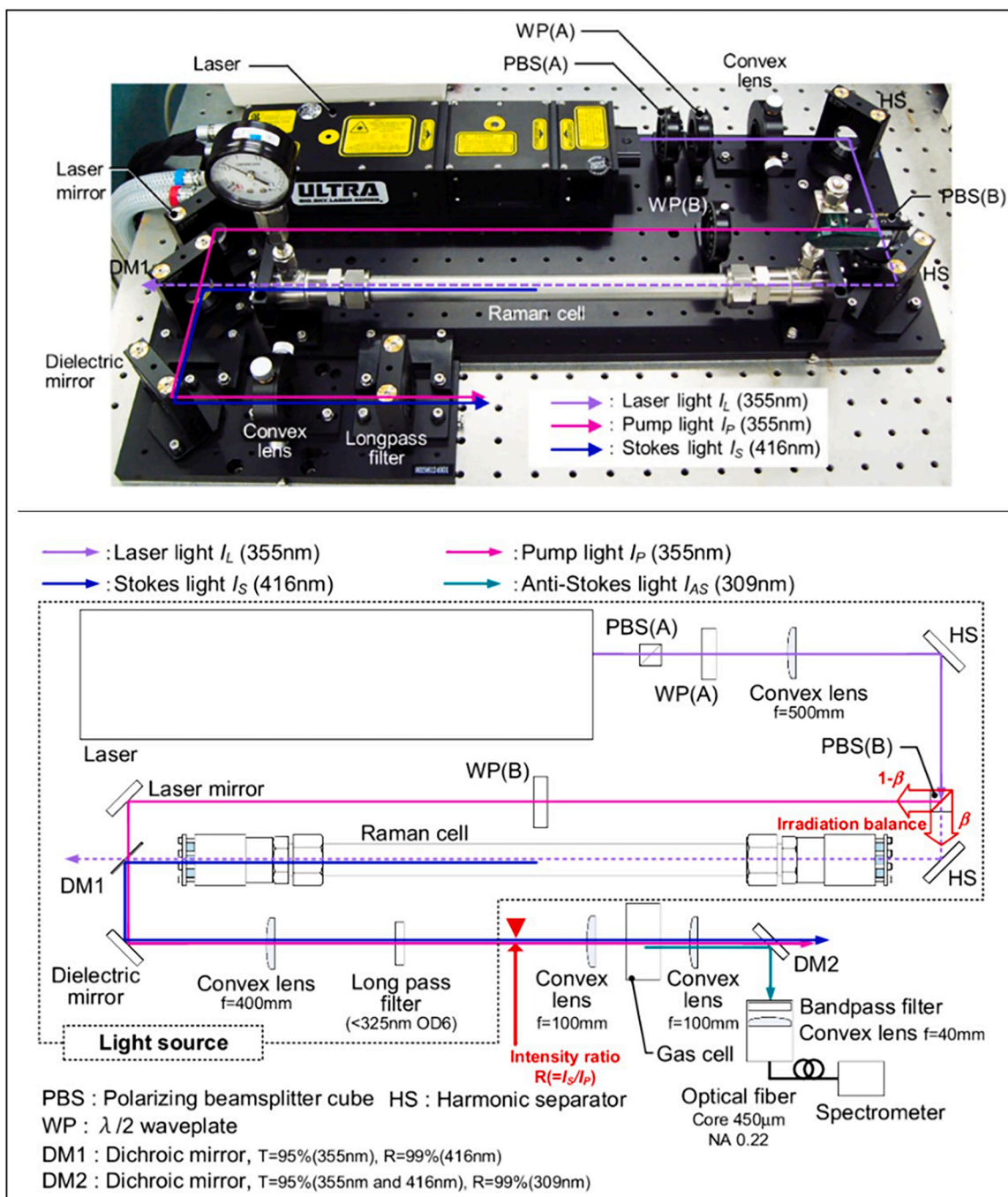


Fig. 8. Optical image and detailed illustration of the light source setup designed by Sugimoto et al. for H_2 leak detection using CARS technique [178].

ppb and selective) of SERS weak-intensity aldehyde molecules by employing a bionic antennae structure, (dendritic Ag nanocrystals). Their study surely paves a path towards the detection of other Raman weak-intensity VOCs by simply investigating the appropriate Raman-active molecules via SERS. Their strategy, having the potential to selectively trick and sensitively SERS detect trace gaseous aldehydes using SERS (even under high moisture conditions), bears every possibility of vast application in the real field and holding an incredible prospect for non-invasive recognition of lung malignancies. Over the years, several SERS-related experimental technologies and techniques that benefit from high electromagnetic field enhancement in plasmonic structures and in nanogaps have been developed for a wide range of applications. Surface-enhanced spatially offset Raman spectroscopy (SESORS) has been advanced in improving signal detection from deeper

sites. With electro-chemical SERS (EC-SERS) molecular resonances can be tuned to the excitation wavelength, providing information about the electronic states involved in SERS. Surface-enhanced hyper Raman scattering (SEHRS) provides complementary vibrational information, due to changed selection rules in multiphoton excitation process.

6.5. Detection using TERS

The TERS technique has the potential to be utilised for the study of small particles or in applications where ultrasensitive spectral analysis is needed. The TERS combines a scanning probe microscopy (SPM) and surface-enhanced Raman scattering to study surface topography at nanoscale level and to generate localised Raman signals. Briefly, incident light of a specific frequency irradiates the tip of the SPM generating

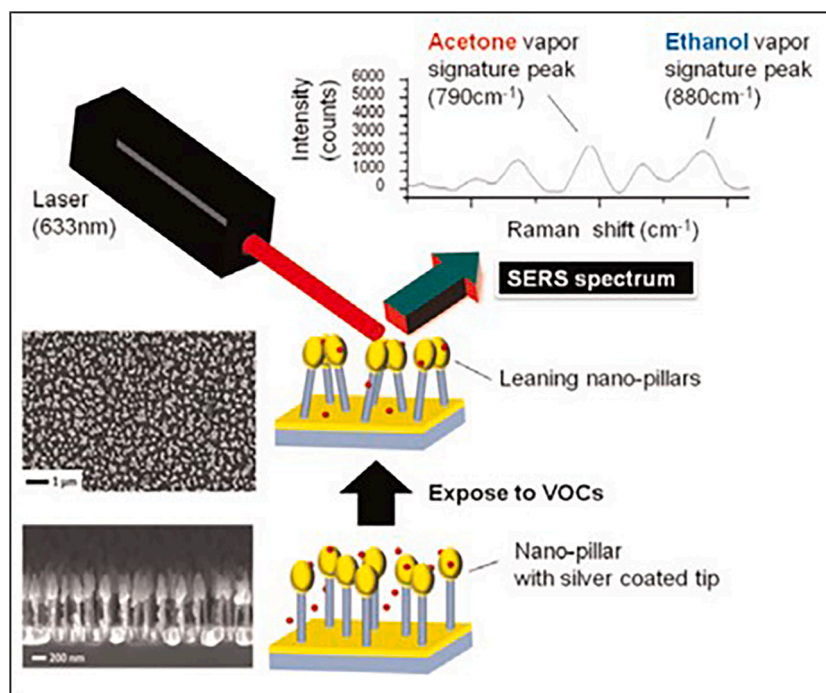


Fig. 9. Pictorial representation of multiplex SERS based VOCs detection with leaning nano-pillar substrate [187]. Reprinted with permission.

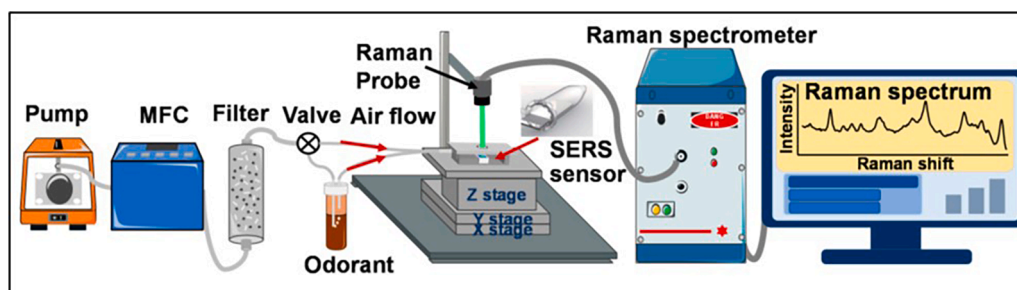


Fig. 10. Schematics of the gas generation and detection system [189].

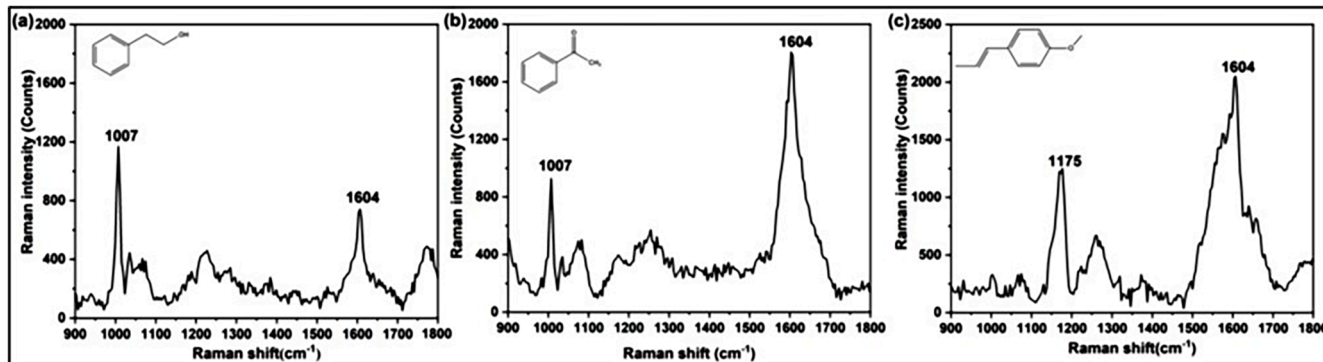


Fig.11. Recorded Raman spectra of (a) phenethyl alcohol gas, (b) acetophenone gas and (c) anethole gas Using the SERS based detection unit [189].

an electromagnetic “hot spot” between the sample surface molecules and the SPM tip. This enhances the Raman signal from the sample molecules close to the “hot spot”. TERS is a highly sensitive technique that can reach a spatial resolution of 1 nm or below [193]. The spatial resolution of TERS is limited to the shape and size of the metal tip apex used [194]. Apart from the SPM tip, the degree of Raman signal enhancement, accuracy, and resolution of the TERS system can be

affected by different design elements including the wavelength and power of the incident light [194], the position of the probe with respect to the sample [194] and direction of incident light electric field component [195]. In addition, the capability of the SPM system can impact the generated Raman signal. The most common SPM techniques adopted for TERS systems are Atomic Force Microscopy (AFM), Scanning Tunneling Microscopy (STM) and Shear Force Microscopy (SFM).

The TERS technique has found applications in a wide range of fields. Park et al. [196] used a TERS imaging technique with ≈ 18 nm spatial resolution to study the properties of grain boundaries, wrinkles and other surface defects in large-area graphene. In a similar study, Sheng et al. [197] utilised a highly sensitive STM-TERS system at high vacuum with a spatial resolution of 0.5 nm to study local vibrational properties of monolayer silicone. They demonstrated a signal enhancement factor of 10 [9]. Apart from structural and topographical studies of 2D materials, TERS has found practical applications in a wider range of fields from biochemistry [198,199] to electrochemistry [198]. Examples of these applications include label-free chemical composition examination in complex biological systems [200], structural organisation studies of large molecules such as collagen fibrils [201] or DNA [202] and investigation of electrochemical reactions at nano scale [203]. One of the limitations of this technique is associated with the short lifetime of the SPM tip, frequent maintenance required for decontamination and lack of reproducible tip fabrication methods [204]. In addition, small shift ($\pm 2-9$ cm^{-1}) [205,206] in the TERS vibrational bands compared to their corresponding bands in surface-enhanced or spontaneous Raman spectra makes TERS spectral interpretation complicated. While the exact nature of this shift is yet to be discovered, it is suggested to be due to the interaction between SPM tip and sample molecules and/or incident light polarization [205,206]. The exponential decay of the electromagnetic field [198] between TERS probe and the sample surface (from the “hot spot”) makes this technique exclusively a surface analysis tool more suitable for liquid and solid samples. Beyond its well-established role in molecular fingerprinting, TERS has demonstrated remarkable capabilities in unravelling the intricacies of adsorbate–substrate interactions, offering insights that are often inaccessible through conventional spectroscopic techniques. For instance, Klingsporn et al. [207] compared the TER spectra of Rhodamine 6G (R6G) on an Ag(111) surface at different temperatures. Theoretical analysis revealed that the observed spectral changes upon cooling were attributed to strong interactions between the ethylamine substituents of R6G and the silver surface. Similarly, Liu et al. [208] employed a “fishing mode” TERS approach to investigate whether a single molecule could bridge the tip-surface junction. The clear correlation between the Raman spectra and measured conductance confirmed TERS’s ability to reveal molecular structures within the tip-sample gap. Additionally, the Weckhuysen [126] and group [126] successfully monitored a photocatalytic reaction using a dual-wavelength TERS approach, highlighting its utility in real-time catalytic studies. Although TERS has not yet been directly applied to gas detection, its inclusion in this context is relevant due to its unique potential to address key limitations encountered by conventional Raman based techniques. TERS offers ultra-high spatial resolution (down to 1 nm) and exceptional signal enhancement, achieved by localizing the electromagnetic field at the apex of a sharp metal tip to create a highly confined “hot spot” [209]. This localised enhancement enables the detection of trace-level analytes with molecular specificity—an essential feature for gas sensing, particularly in environments where ultra-low concentration detection and insights into molecular-level interactions are critical. The ability of TERS to detect trace quantities of analytes adsorbed on functionalised surfaces or catalytic sites, potentially down to the single-molecule level, holds significant promise. Given that many gas-sensing mechanisms rely on surface interactions (e.g., adsorption on catalysts, nanostructures, or sensor interfaces), TERS can provide localised chemical insights at these active sites. This capability facilitates a deeper understanding of gas-solid interactions in real-time, which is invaluable for the development of next-generation gas sensors. Furthermore, TERS can spatially resolve chemical changes on sensor surfaces, offering detailed insights into heterogeneous reactions, catalyst activity, and degradation processes at the nanoscale which are key factors to design and optimise gas sensors and their corresponding performance. While current limitations, such as tip stability, spectral shifts, and the exponential decay of the electromagnetic field between the TERS probe and the sample surface, have confined its primary

applications to liquids and solids, the rapid advancements in probe design, tip fabrication, and system integration suggest that TERS could be effectively adapted for gas-phase studies in the near future. The surface sensitivity of this technique, could become an advantage when targeting adsorbed gas species or investigating interfacial phenomena to understand site specific chemical reactivity within micro- and even nano-environments for the development of desired gas sensors.

7. Commercial/Industrial adaptation of Raman-based gas sensor techniques

Raman has been used for many years as a materials analysis tool but developments over the past two decades have seen it be used for an extended branch of liquids and gases. This is primarily due to the advancements in surface and waveguide enhancement techniques that allow for the signal intensity to increase dramatically. In industry the dominant spectroscopic technique is FTIR however other techniques must be used in tandem to measure O_2 which is required for environmental permits and process information. Early applications of Raman spectroscopy using enhancement (either surface or waveguide) focus on medical applications in a ‘cleaner’ environment without interference from excessive vibration or problematic gases. Schlüter et al [210] measured volatile anaesthetics (sevoflurane, desflurane and isoflurane) and some common gases (N_2 , N_2O , O_2 and CO_2) by Raman spectrometer to monitor concentration. This study was shown to have close values to comparative gas chromatography (GC) measurements for N_2 , N_2O and O_2 . Industrial applications were developed in 2014 [135] however, Kiefer et al. [132] demonstrated the idea in 2008 for gas turbine and biogas inlet analysis. Kiefer et al installed the Raman sensor at a combined cycle gas turbine (CCGT) power plant in Karlsruhe, Germany and monitored natural gas composition and ambient gases from the supply line. They reported that in these environments the probe and spectrometer was under significant stress due to constant mechanical vibration and higher ambient temperature. However, given these challenges, alongside a GC the instrument performed very accurately and with a 30 s measurement interval when compared to the 30 min interval for the GC. Many other natural gas applications have been described in addition to this [130,144,211] which was adapted to biogas plant [212] analysis of CH_4 , N_2 , O_2 and CO_2 from anaerobic digestion. Sieburg et al [212] was able to find accurate concentrations of CH_4 , N_2 , O_2 and CO_2 in a miniaturised biogas fermentation plant. Whilst not a full-scale plant, diagrams show that the key components were kept accurate and therefore this demonstrates applicability for scaling up to full size industrial biogas plants. A study conducted by Hansen, S [213] installed a Raman probe at the Nybro natural gas plant in Denmark for hydrocarbon, nitrogen and oxygen analysis comparing results with gas chromatography. In addition, they also took gas samples from several other extraction and storage plants to monitor the previous compounds, hydrogen sulphide and poly-isobutane with difficulty being reported for monitoring of isobutane compounds due to microdroplet formation. However, most other hydrocarbons (particularly methane) showed a good accuracy with the compared measured GC value.

Commercially available Raman probes for gas monitoring are few and far between however current suppliers include HORIBA, tec5USA [211] and Ocean Insight. These are currently unaccredited for environmental monitoring however there is an ISO standard [214] for application in upstream quantifying of natural gas therefore most commercial efforts are focussed on this area. Tec5USA have a commercially available system specifically for the natural gas industry’s process control, quality assurance and optimising feed input. These are fixed units that continuously monitor to provide time dependant analysis of input, output and bypass concentration of hydrocarbons and H_2S . Ocean Insight (formally Ocean Optics) supply a portable Raman probe that is quoted as being able to monitor gases [215] it is of note that this instrument does not use any fibre enhancement. This product however does not have any readily available case studies for gas analysis. Table 2

Table 2
Practical implementation/installation of Raman-based sensors.

Case Study	Application	Year Of Installation	Notes
Hansen, S et al. [213]	Natural Gas	2000	Hydrocarbon analysis at Nybro plant inlet Torup Gas Storage Facility
	Natural Gas	2000	
Kiefer et al. [132] Schlüter et al. [132]	Natural Gas	2008	CCGT Volatile anaesthetics
	Medical	2012	
Keiner et al. [132]	Environmental	2014	Carbon isotope labelling
Sieburg et al. [212]	Natural Gas	2018	Miniaturised biogas plant
AZO Materials, tecSUSA [211]	Natural Gas / Environmental	2021	Commercial installation

is a better representative of the overall topic.

8. Critical analysis and conclusion

This review offers a comprehensive discussion on advanced methodologies for Raman spectroscopy focusing on applications relevant to gas sensor research. The techniques encompass SRS, StRS, CARS, SERS, and TERS, discussing both their individual advantages and limitations. By addressing recent studies, novel developments (both at lab and industrial scale), and the underlying principles of each technique, this review provides readers with a foundational understanding, critical insights, and a current viewpoint on the field. The APPENDIX section includes the detailed theoretical knowledge base for deeper understanding and reference. The value of Raman spectroscopy in gas sensing is evident and its capacity towards high specificity and sensitivity, especially when enhanced by advanced methods, continues to push the boundaries of detection capabilities/strategies. In the context of gas sensors, the methods analysed here show distinct characteristics that position them uniquely within the scientific and industrial landscape, particularly as they relate to their practical adoption. Each of these advanced Raman techniques brings significant advantages, whether through enhanced sensitivity, increased resolution, or the ability to operate in real-time, yet practical limitations persist in terms of deployment and scalability.

Briefly, StRS and CARS demonstrate the potential for high-speed detection with amplified signal strengths, making them highly suitable for real-time monitoring. SRS holds promise for high sensitivity, allowing analyte detection even at low concentrations, which is crucial in gas sensing. However, both SRS and CARS require complex instrumentation and intricate setup procedures, which could impede their practical use in field applications and in resource-limited settings. Their complexity also necessitates skilled operators and precise alignment, potentially restricting their wider adoption in non-specialist environments. SERS has drawn attention for the scope of increased sensitivity through plasmonic enhancements and ability to detect trace levels of gas molecules when paired with suitable substrate designs, making it particularly attractive for applications (majorly biological/biosensing) demanding high sensitivity. Yet, SERS's dependency on specialised nanostructured substrates introduces a level of variability and reproducibility challenges. Moreover, substrate degradation and the complexity of producing consistent, reproducible surfaces at scale remain technical obstacles. For practical large-scale use, developing more robust and reproducible SERS substrates will be essential to overcoming these limitations. TERS offers nanoscale resolution which is an unparalleled advantage when molecular-level insight is necessary and it offers a unique opportunity for fundamental research in gas sensing, especially for applications requiring spatial resolution beyond the diffraction limit. However, its reliance on precision-engineered scanning probe systems limits its utility in routine gas sensing,

especially for daily based industrial applications. TERS also necessitates highly controlled experimental conditions and is predominantly useful within laboratory settings, thus limiting its application in broader, field-based applications. While SERS dominates the field in terms of innovative detection strategies, FERS and WGRS (which operates on SRS) emerge as more scalable alternatives for gas sensing applications. These techniques involve guiding the laser excitation through optical fibres or waveguides, offering several practical benefits that align well with the demands of industrial and environmental monitoring. Specifically, the ability to collect signals over extended distances allows for remote, in situ measurements—a feature that is highly desirable in real-world gas sensing applications where direct access to the sensing environment may be challenging or hazardous. Additionally, the relative ease of integration with existing fibre-optic systems makes FERS and WGRS suitable for incorporation into established sensing infrastructures, potentially facilitating broader adoption across various sectors. A significant advantage of SRS based FERS/WGRS lies in their comparatively simpler setup requirements. Unlike the high precision needed for techniques like TERS, which relies on scanning probe systems, FERS/WGRS can operate with minimal alignment and lower maintenance, increasing their practicality for both laboratory and field applications. Furthermore, the adaptability of optical fibres to harsh conditions and high temperatures enhances their suitability for environments where traditional optical components might fail. This resilience, coupled with the capability for continuous, real-time monitoring, presents a compelling case for SRS based FERS/WGRS in industrial gas sensing. However, FERS/WGRS are not without limitations. The reliance on optical fibres introduces potential issues with signal attenuation and scattering losses over long distances, which can reduce sensitivity, particularly for trace-level detection. Additionally, the effectiveness of this emerging technology is currently constrained by the quality of fibre materials, which must be further optimised to improve durability and reduce background interference. Nevertheless, advances in fibre manufacturing and coating techniques hold promise for addressing these issues, suggesting that SRS could become highly viable alternatives for large-scale gas sensing through its adoption via FERS/WGRS. The broader adoption of Raman-based gas sensing in industrial applications will ultimately depend on advancements that can address scalability, cost, and durability. As demonstrated, each of the techniques discussed has unique strengths, but also practical challenges that need to be mitigated. A particularly promising direction lies in hybrid approaches that combine elements from different Raman methodologies. For example, integrating SERS with FERS could enhance sensitivity while enabling remote sensing capabilities, potentially overcoming the reproducibility challenges associated with SERS substrates while retaining the advantages of fibre-based delivery. Future research should focus on the development of more durable, reproducible, and cost-effective substrates for SERS, as well as enhancements to the material quality and structural integrity of optical fibres used in FERS/WGRS through SRS. Advanced materials, such as robust polymers or specially engineered nanostructures, could play a significant role in enhancing the resilience of these components under varying environmental conditions. Additionally, the incorporation of machine learning algorithms for signal processing holds potential for improving the accuracy and interpretability of Raman spectra, particularly for complex gas mixtures where overlapping signals may complicate analysis. Authors found that the adoption of SRS as a primary method in gas sensing will also benefit from further standardisation of fibre design and performance parameters, enabling broader compatibility with existing industrial systems. Collaborative efforts between academia and industry will be essential in driving these advancements, particularly in the testing and validation of these systems under real-world conditions. Furthermore, regulatory frameworks and standardisation bodies could play a key role in establishing guidelines for the quality, safety, and environmental impact of Raman-based gas sensing technologies, potentially accelerating their integration into routine industrial practice. In conclusion, Raman spectroscopy, bolstered by advanced

techniques such as SRS, CARS, SERS, and TERS, provides a multifaceted toolkit for gas sensing applications. While SERS stands out for its sensitivity, especially for trace detection, the practical benefits of SRS based FERS/WGRS make it a strong candidate for large-scale implementation. A continued focus on addressing the reproducibility, durability, and cost-efficiency challenges associated with these techniques will be crucial for advancing Raman-based gas sensors towards industrial use. The trajectory of future research must balance the pursuit of fundamental improvements with practical considerations, fostering innovations that are not only academically significant but also viable for widespread industrial adoption. The insights provided in this review underscore the need for interdisciplinary collaboration, strategic investment, and a forward-looking approach to ensure that Raman spectroscopy can fulfil its potential as a transformative tool in the field of gas sensing.

CRedit authorship contribution statement

Deblina Majumder: Writing – review & editing, Writing – original draft, Software, Project administration, Methodology, Investigation,

Appendix

The Raman shift, which reflects the energy difference between the incident and scattered photons, may be calculated using the following equation [95]:

$$\Delta\nu(\text{cm}^{-1}) = \left(\frac{1}{\lambda_0(\text{nm})} - \frac{1}{\lambda_1(\text{nm})} \right) \times (10^7 \text{nm}) / (\text{cm}) \quad (9)$$

From spectroscopic point of view, the scattered radiation has a frequency of $\mu_0 - \mu_m$, where μ_m is the molecular frequency. Similarly, there is a chance that molecules in excited vibrational or rotational state will give up energy to the light beam; in this case, the scattered radiation will have a higher frequency ($\mu_0 + \mu_m$). Thus, three lines in the scattered radiation may be observed: (i) one line at μ_0 , corresponding to the Rayleigh scattering; and two Raman Lines, (ii) one at ($\mu_0 + \mu_m$), the anti-stokes line and (iii) ($\mu_0 - \mu_m$), the Stokes line.

Classical theory of Raman spectroscopy

If a molecule is put in a static electric field, it suffers from some distortion [216]. There occurs a charge separation, which causes an induced dipole moment to be set up in the molecule and the molecule is said to be polarized. Let ' μ ' be the dipole moment induced by the electric field E, then, $\mu \propto E$

$$\mu = \alpha E \quad (10)$$

Where ' α ' is the proportionality constant and is known as polarisability of the molecule and it is molecule specific. If $E = 1$, $\mu = \alpha$, thus α is defined as the amount of induced dipole moment by a unit electric field.

Dipole moment is a molecular property [217], and the extent of dipole moment is proportional to the electron displacement cloud. Polarisability of a molecule is represented by a 3D geometry which is known as polarisability ellipsoid. Greater the polarisability of the molecule, smaller will be the size of polarisability ellipsoid. Due to the polarisability effect on Raman signal, there lie certain conditions for a molecule to be Raman active. For microwave activity a molecule must be polar. For IR activity there must be a change in moment during vibration. All molecules are UV visible active since there is change in electron distribution and this causes change in dipole moment [218,219]. For Raman activity of a molecule, there must be a change in polarisability during rotation or vibration. This is the key parameter of every molecule being Raman active. Following are the conditions, (i) change in polarisability means a change in shape and size in polarisability ellipsoid, (ii) Or change in direction of polarisability ellipsoid, or (iii) both [145]. This change in polarisability ellipsoid (even instantaneous) makes even the diatomic molecules (such as, O₂, N₂ etc) Raman active while that is restricted in case of IR spectra as they do not have any bonds and therefore no stretching/bending frequencies could occur. Under alternating electric vector (Electric vector of light), it can be represented by the following equation (11). [220]

$$E = E_0 \sin 2\pi\mu_0 t \quad (11)$$

Where, E_0 = amplitude of the electric vector, μ_0 = frequency, leading to the following correlation as shown equation (12).

$$\mu = \alpha E_0 \sin 2\pi\mu_0 t \quad (12)$$

Polarisability of a molecule must be a function of displacement during the course of vibration or rotation, and hence formulated in equation (13) [221].

$$\alpha = \alpha_0 + \left(\frac{d\alpha}{dq} \right) q \quad (13)$$

Where, α_0 represents polarisability at eqm of the molecule. $\left(\frac{d\alpha}{dq} \right)$ is gradient of polarisability with respect to displacement co-ordinate, q and can be formulated as below in equation (14).

Data curation, Conceptualization. **Ronak Janani:** Writing – original draft. **Alex Scrimshire:** Writing – original draft. **Alex Stone:** Writing – review & editing. **William Brooks:** Funding acquisition. **Chris Holcroft:** Funding acquisition. **Rob Werner:** Funding acquisition. **Spencer Green:** Project administration. **Natalie Wheeler:** Project administration, Funding acquisition. **Paul . A . Bingham:** Project administration, Funding acquisition.

Declaration of competing interest

The authors declare that they have no known competing financial interests or personal relationships that could have appeared to influence the work reported in this paper.

Acknowledgements

The authors would like to thank all the project partners at IS-Instruments, University of Southampton, Glass Technology Services, Breedon Group, and Wienerberger. This work was funded by Innovate UK (GRIFFIN, 95372).

$$\mu = \left\{ \alpha_0 + \left(\frac{d\alpha}{dq} \right) q \right\} E_0 \sin 2\pi\mu_0 t; \quad (14)$$

Where again, 'q' is a time dependent quantity, and it can be expressed as follow (equation 15), $q = q_0 \sin 2\pi\mu_m t$ — — — (15); Where, μ_m is molecular frequency, and where, q_0 is amplitude of vibration. Thus now, ' μ ' can be derived and presented as shown below.

$$\begin{aligned} \mu &= \left\{ \alpha_0 + \left(\frac{d\alpha}{dq} \right) q_0 \sin 2\pi\mu_m t \right\} E_0 \sin 2\pi\mu_0 t \\ &= \alpha_0 E_0 \sin 2\pi\mu_0 t + \frac{1}{2} \left(\frac{d\alpha}{dq} \right) q_0 2 (\sin 2\pi\mu_m t \cdot \sin 2\pi\mu_0 t) E_0 \\ \therefore \mu &= \alpha_0 E_0 \sin 2\pi\mu_0 t + \frac{1}{2} \left(\frac{d\alpha}{dq} \right) q_0 E_0 \cos 2\pi(\mu_0 - \mu_m)t - \frac{1}{2} \left(\frac{d\alpha}{dq} \right) q_0 E_0 \cos 2\pi(\mu_0 + \mu_m)t \end{aligned} \quad (16)$$

Thus, dipole moment oscillates with three distinct frequencies:

(i) μ_0 with amplitude $\alpha_0 E_0$

(ii) $(\mu_0 - \mu_m)$ & $(\mu_0 + \mu_m)$ with much smaller amplitude $\frac{1}{2} \left(\frac{d\alpha}{dq} \right) q_0 E_0$

Hence, this results relatively intense beam at one frequency (Rayleigh scattering), and two very weak beam at frequency, slightly above (anti-Stokes) and slightly below (Stokes), the intense one. This is how a Raman signal can be recorded [15]. Concluding that the only selection rule for molecules to be Raman active is the requirement of change in polarisability of the molecule occurs during its normal modes. As it is well known that polarisability of a molecule is the ease with which the electron cloud of a molecule can be altered under electromagnetic field or simply by irradiating with light source. Here comes the classical concept of Raman spectroscopy [84] to be utilised as an analytical tool by using this source of light as a probe towards the target analytes, especially in case of gas substances. Considering the continuous motion of molecules by vibrations, rotations, and translations, they are prone to offer an instantaneous change in associate dipoles or electron clouds. Even though the actual vibration of a molecule seems random, but the superposition principle of some simple vibration modes is termed as normal mode and each of these normal modes has its own frequency. The vibrations of a molecule are thus often represented by its normal modes and each absorption in a vibrational spectrum corresponds to a normal mode. Such as, the four normal modes of carbon dioxide, are shown below in Fig. 2(c) and they are the symmetric stretch, the asymmetric stretch and two bending modes. The two of the bending modes have the same energy and differ only in their corresponding direction of the associated bending motion. Modes, having the same energy are termed as degenerate. In the classical treatment of molecular vibrations, each normal mode is considered as a simple harmonic oscillator. An atom holds 3 degrees of freedom (x, y and z direction). Hence, a molecule containing N atoms has 3N degrees of freedom: 3 translations, 3 rotations (2 for a linear molecule) and 3N-6 normal modes (3N-5 is for linear molecules) [222]. Considering the case of a diatomic molecule, e.g., the stretch to alter the electron cloud will be different for the three vibration states of its harmonic vibration having frequency ν_v , as schematically shown in Fig. 2(d). It is evident that in case of longer the bond distance, the electrons are pushed apart from the nuclei and thus resulting easier their movement at ease. This change in ease with which the electron cloud of a molecule can be distorted (i.e., change in polarisability) is responsible for Raman activity. Quantum mechanics and the group theory can further explain or determine the contribution of normal modes of complex molecules towards their change in polarisability [223]. Upon irradiation with a light source/electromagnetic field, a typical Raman spectrum of any target molecule displays the difference in frequencies between the incident radiation and the scattered radiation, which is expressed as wavenumbers, versus the intensity (I) of the scattered radiation. In the recent time, the following equation is used to calculate and correlate the Raman intensity during a particular vibration [224]:

$$I = cte(\nu_0 + \nu_v/\nu_v)^4 * \frac{NI_0}{\left(1 - e^{-\frac{h\nu_v}{kT}}\right)} \left\{ 45(\alpha^s)^2 + 13(\alpha^a)^2 \right\} \quad (17)$$

Here, ν_0 is the frequency of the incident light, ν_v is the frequency of vibration of the molecule, N is the number of irradiated Raman active molecules, I_0 is the power of the light source, h is Planck's constant ($=6.6260 \times 10^{-34}$ J s), k is the Boltzman's constant, T is temperature, α^s is the polarizability from the molecules causing Stokes radiation, and α^a is the polarizability from the molecules causing anti-Stokes radiation [225].

Quantum consideration of Raman spectroscopy

Quantum Consideration on Raman Effect includes Rotational and Vibrational Raman spectra. In case of linear molecule, rotational energy level expression is given by

$$\epsilon_J = BJ(J+1)cm^{-1} \quad (18)$$

for pure microwave spectroscopy. The selection rule is

$$\Delta J = \pm 1 \quad (19)$$

(J= rotational quantum number). For rotational Raman transition, the selection rule is $\Delta J = 0, \pm 2$; When $\Delta J = 0$, leading to Rayleigh scattering. If, $\Delta J = \pm 2$, Raman scattering occurs. In general, for rotational Raman transition, energy separation between the rotational levels is obtained as follows,

$$\Delta \epsilon = \epsilon_{J+2} - \epsilon_J \quad (20)$$

[where J = smaller quantum number] and which ultimately deducing to the following equation, where,

$$\Delta\varepsilon = B[4J + 6]cm^{-1}. \quad (21)$$

To avoid any confusion, it must be mentioned that 'cm⁻¹' is being used as the corresponding unit throughout the article. Thus, Raman lines correspond to the wave numbers, -

$$\bar{\nu}_{spect} = \bar{\nu}_0 \pm B(4J + 6)cm^{-1} \quad (22)$$

Here, '+' sign stands for anti-Stokes lines and '-' sign stands for Stokes lines. From the determined value of B, the characteristic molecular radius of any species can be calculated. This is the most unique advantage of Raman spectroscopy to provide the corresponding molecular fingerprint.

In case of Vibrational Raman spectroscopy, the change in polarisability of the molecule is considered during vibrational motion. As a result, the molecule, may be Raman active. Energy expression for vibrational levels is given by [102]:

$$\varepsilon_v = \left(v + \frac{1}{2} \right) \bar{\omega}_e \kappa_e cm^{-1} \quad (23)$$

Where, 'v' is 0,1,2,3..., 'κ_e' is anharmonicity constant, 'a' is a small positive quantity, and 'ω_e' is (hypothetical) eqm oscillation frequency. The selection rule for vibrational Raman transition is same as that of simple vibrational transition [107], and which is as follows, Δv = ±1, ±2, ±3...

In this case, Δv = 0 is also allowed which produces Rayleigh scattering. According to selection rule, Raman lines will be observed at the frequencies, obeying the following equation/relation:

$$\bar{\nu}_{spec} = \bar{\nu}_0 \pm \Delta\varepsilon \quad (24)$$

Here, '+' sign stands for anti-Stokes lines and '-' sign stands for Stokes lines and corresponding spectral lines will be observed at the following frequencies (numbered below from i-iv), presented with the way of calculating them [102].

$$1) \bar{\nu}_{spect} = \bar{\nu}_0 \pm \Delta\varepsilon_{fundamental} = \bar{\nu}_0 \pm (1 - 2\kappa_e)\bar{\omega}_e cm^{-1} - - - (25)$$

$$2) \bar{\nu}_{spect} = \bar{\nu}_0 \pm \Delta\varepsilon_{first\ overtone} = \bar{\nu}_0 \pm (1 - 3\kappa_e)2\bar{\omega}_e cm^{-1} - - - (26)$$

$$3) \bar{\nu}_{spect} = \bar{\nu}_0 \pm \Delta\varepsilon_{2nd\ overtone} = \bar{\nu}_0 \pm (1 - 4\kappa_e)3\bar{\omega}_e cm^{-1} - - - (27)$$

$$4) \bar{\nu}_{spect} = \bar{\nu}_0 \pm \Delta\varepsilon_{hot\ band} = \bar{\nu}_0 \pm (1 - 4\kappa_e)\bar{\omega}_e cm^{-1} - - - (28)$$

Data availability

Data will be made available on request.

References

- [1] H.B. Lemon, Spectroscopic studies on hydrogen, *Astrophys. J.* 35 (1912) 109.
- [2] F. Röck, N. Barsan, U. Weimar, Electronic nose: current status and future trends, *Chem. Rev.* 108 (2008) 705–725.
- [3] B.H.B.H. Stuart, Industrial and environmental applications. *Infrared Spectroscopy: Fundamentals and Applications*, 2004, pp. 167–186, <https://doi.org/10.1002/0470011149.ch8>.
- [4] Scientific, T. F. Model 410i carbon dioxide gas analyzer. Thermo Scientific™ Preprint at <https://www.thermofisher.com/order/catalog/product/410i#/410i> (2021).
- [5] S. Wu, G. Lv, R. Lou, Applications of chromatography hyphenated techniques in the field of lignin pyrolysis, in: R. Davarnejad, M. Jafarkhani (Eds.), *Applications of Gas Chromatography*, IntechOpen, 2012, <https://doi.org/10.5772/32446>. Ch. 3.
- [6] Portable Gas Analyzers. Gasetm Preprint at <https://www.gasetm.com/products/category/portable-gas-analyzers/>.
- [7] ARCOptix GASEX OEM. ARCOptix Preprint at https://www.arcoptix.com/Gas_analyzer.htm.
- [8] Heard, D. E. et al. Frontmatter. in *Analytical Techniques for Atmospheric Measurement i–xvii* (2006). doi:<https://doi.org/10.1002/9780470988510.fmatter>.
- [9] L.B. Mendes, et al., NDIR gas sensor for spatial monitoring of carbon dioxide concentrations in naturally ventilated livestock buildings, *Sensors* 15 (2015), <https://doi.org/10.3390/s150511239>. Preprint at.
- [10] R. Rubio, et al., Non-selective NDIR array for gas detection, in: *Smart Sensors, Actuators, and MEMS II*, 5836, 2005, pp. 239–246.
- [11] Q. Tan, et al., Three-gas detection system with IR optical sensor based on NDIR technology, *Opt. Lasers. Eng.* 74 (2015) 103–108.
- [12] SIEMENS. SIPROCESS GA700 – the latest generation of continuous process gas analytics. Preprint at <https://new.siemens.com/global/en/products/automation/process-analytics/extraktive-continuous-process-gas-analytics/siprocess-ga700.html> (2021).
- [13] T. Lillesand, R.W. Kiefer, J. Chipman, *Remote Sensing and Image Interpretation*, Wiley, 2015.
- [14] D. Popa, F. Udrea, Towards integrated mid-infrared gas sensors, *Sensors* 19 (2019), <https://doi.org/10.3390/s19092076>. Preprint at.
- [15] C.V Raman, K.S Krishnan, A new type of secondary radiation, *Nature* 121 (1928) 501–502.
- [16] G. Harry Poole, Structure of benzene. Part XV. Experimental methods for Raman spectroscopy, including a Micro-method. Revision of the Raman spectrum of Hexad eut erobenzene, *R. Soc. Chem.* 245–252 (1946).
- [17] B.D. Saksena, Raman effect and crystal symmetry, *Proc. Indian Acad. Sci. - Section A* 11 (1940) 229–245.
- [18] G. Eckhardt, D.P. Bortfeld, M. Geller, Stimulated emission of stokes and anti-Stokes Raman lines from diamond, calcite, and α-sulfur single crystals, *Appl. Phys. Lett.* 3 (1963) 137–138.
- [19] Rasetti, F. Interview with Franco Rasetti. Preprint at (1982).
- [20] A. Weber, *Raman Spectroscopy of Gases and Liquids*, 11, Springer Science & Business Media, 2012.
- [21] K. Kneipp, H. Kneipp, I. Itzkan, R.R. Dasari, M.S. Feld, Ultrasensitive chemical analysis by Raman spectroscopy, *Chem. Rev.* 99 (1999) 2957–2975.
- [22] T.De Beer, et al., Near infrared and Raman spectroscopy for the in-process monitoring of pharmaceutical production processes, *Int. J. Pharm.* 417 (2011) 32–47.
- [23] C. Rathmell, D. Chen, Data-driven Raman spectroscopy in oil and gas: rapid online analysis of complex gas mixtures, *Spectroscopy* 33 (2018) 34–42.
- [24] S. Hanf, T. Bögözi, R. Keiner, T. Frosch, J. Popp, Fast and highly sensitive fiber-enhanced Raman spectroscopic monitoring of molecular H₂ and CH₄ for point-of-care diagnosis of malabsorption disorders in exhaled human breath, *Anal. Chem.* 87 (2015) 982–988.
- [25] T. Jochum, L. Rahal, R.J. Suckert, J. Popp, T. Frosch, All-in-one: a versatile gas sensor based on fiber enhanced Raman spectroscopy for monitoring postharvest fruit conservation and ripening, *Analyst* 141 (2016) 2023–2029.
- [26] P.W Atkins, *Physical Chemistry*. Physical Chemistry, Peter W., Paula, J. De & Keeler, J. Atkins', Oxford University Press, 2018.
- [27] A. Weber, S.P.S. Porto, L.E. Cheesman, J.J. Barrett, High-resolution Raman spectroscopy of gases with CW-laser excitation*, *J. Opt. Soc. Am.* 57 (1967) 19–28.
- [28] Toledo, M. Raman vs. IR spectroscopy. 1 Preprint at (2022).
- [29] J. Heland, K. Schäfer, Determination of major combustion products in aircraft exhausts by FTIR emission spectroscopy, *Atmos. Environ.* 32 (1998) 3067–3072.
- [30] E. Puckrin, W.F.J. Evans, T.A.B. Adamson, Measurement of tropospheric ozone by thermal emission spectroscopy, *Atmos. Environ.* 30 (1996) 563–568.
- [31] B.A. Eckenrode, Environmental and forensic applications of field-portable GC-MS: an overview, *J. Am. Soc. Mass Spectrom.* 12 (2001) 683–693.
- [32] D.-W. You, et al., A portable gas chromatograph for real-time monitoring of aromatic volatile organic compounds in air samples, *J. Chromatogr. A* 1625 (2020) 461267.
- [33] F.M. Hoffmann, Infrared reflection-absorption spectroscopy of adsorbed molecules, *Surf. Sci. Rep.* 3 (1983) 107–192.
- [34] L.B. Kreuzer, Ultralow gas concentration infrared absorption spectroscopy, *J. Appl. Phys.* 42 (1971) 2934–2943.
- [35] E. Stark, K. Luchter, M. Margoshes, Near-infrared analysis (NIRA): a technology for quantitative and qualitative analysis, *Appl. Spectrosc. Rev.* 22 (1986) 335–399.

- [36] A. Rosenzweig, P.R. Griffiths, Photoacoustics and photoacoustic spectroscopy, *Phys. Today* 34 (1981) 64–66.
- [37] J. Laufer, D. Delpy, C. Elwell, P. Beard, Quantitative spatially resolved measurement of tissue chromophore concentrations using photoacoustic spectroscopy: application to the measurement of blood oxygenation and haemoglobin concentration, *Phys. Med. Biol.* 52 (2007) 141–168.
- [38] A. Rosenzweig, Photo-acoustic spectroscopy of solids, *Rev. Sci. Instrum.* 48 (1977) 1133–1137.
- [39] G. Berden, R. Peeters, G. Meijer, Cavity ring-down spectroscopy: experimental schemes and applications, *Int. Rev. Phys. Chem.* 19 (2000) 565–607.
- [40] D.E. Canfield, A.N. Glazer, P.G. Falkowski, The evolution and future of earth's nitrogen cycle, *Science* (1979) 330 (2010) 192–196.
- [41] E.R. Crosson, et al., Stable isotope ratios using cavity ring-down spectroscopy: determination of $^{13}\text{C}/^{12}\text{C}$ for carbon dioxide in human breath, *Anal. Chem.* 74 (2002) 2003–2007.
- [42] M.S. Murphy, M. Sood, T. Johnson, Use of the lactose H₂ breath test to monitor mucosal healing in coeliac disease, *Acta Paediatr.* 91 (2002) 141–144.
- [43] D. Patil, A brief review on gas chromatography, *Asian J. Pharmaceut. Anal.* 47–52 (2023), <https://doi.org/10.52711/2231-5675.2023.00008>.
- [44] G. Gross, V. Reid, R. Synovec, Recent advances in instrumentation for gas chromatography, *Curr. Anal. Chem.* 1 (2005) 135–147.
- [45] E. Matisová, M. Dömötörová, Fast gas chromatography and its use in trace analysis, *J. Chromatogr. A* 1000 (2003) 199–221.
- [46] E. Chatton, et al., Field continuous measurement of dissolved gases with a CF-MIMS: applications to the physics and biogeochemistry of groundwater flow, *Environ. Sci. Technol.* 51 (2017) 846–854.
- [47] B.J. Pollo, G.L. Alexandrino, F. Augusto, L.W. Hantao, The impact of comprehensive two-dimensional gas chromatography on oil & gas analysis: recent advances and applications in petroleum industry, *TrAC Trends Analyt. Chem.* 105 (2018) 202–217.
- [48] B. Daham, et al., Application of a portable FTIR for measuring on-road emissions. SAE Technical Paper, 2005, <https://doi.org/10.4271/2005-01-0676>.
- [49] M. Frey, et al., Calibration and instrumental line shape characterization of a set of portable FTIR spectrometers for detecting greenhouse gas emissions, *Atmos. Meas. Tech.* 8 (2015) 3047–3057.
- [50] F. Hase, et al., Application of portable FTIR spectrometers for detecting greenhouse gas emissions of the major city Berlin, *Atmos. Meas. Tech.* 8 (2015) 3059–3068.
- [51] Gaset. GT5000 Terra – Splashproof multigas FTIR analyzer. <https://www.gasmet.com/products/category/portable-gas-analyzers/gt5000-terra/>.
- [52] Gaset. DX4015 – portable analyzer for humid conditions. <https://www.gasmet.com/products/category/portable-gas-analyzers/dx4015/>.
- [53] R. Bajgain, X. Xiao, J.B. Basara, J.L. Steiner, Soil greenhouse gas (CO₂, N₂O and CH₄) flux measurements from grazing pastures using automated system, in: AGU Fall Meeting Abstracts 2018 B21K-2490, 2018.
- [54] GASEX PORTA Portable Gas Analysis System. ACTTR.
- [55] J.–C. Meraz, L.–K. Meredith, J.–L.–M. Van Haren, T.–H.–M. Volkman, Measuring volatile organic compounds and stable isotopes emitted from trees and soils of the Biosphere 2 Rainforest, in: AGU Fall Meeting Abstracts 2017 B43A-2109, 2017.
- [56] C. Zhou, B. Zhang, C. Mu, Z. Chu, L. Sun, Multi-objective optimization considering cost-benefit ratio for the placement of gas detectors in oil refinery installations, *J. Loss. Prev. Process. Ind.* 62 (2019) 103956.
- [57] T.-V. Dinh, I.-Y. Choi, Y.-S. Son, J.-C. Kim, A review on non-dispersive infrared gas sensors: Improvement of sensor detection limit and interference correction, *Sens. Actuat. B Chem.* 231 (2016) 529–538.
- [58] IRIDIAN. Clear the air: new optical filters for sensors and detectors. Preprint at https://www.irdian.ca/wp-content/uploads/2021/04/optical_filters_for_sensors_and_detectors.pdf.
- [59] F. Carotenuto, et al., Long-term performance assessment of low-cost atmospheric sensors in the arctic environment, *Sensors* 20 (2020).
- [60] A.I. Herts, I.M. Tsidylo, N.V. Herts, S.T. Tolmachev, Cloud service ThingSpeak for monitoring the surface layer of the atmosphere polluted by particulate matters, CTE Workshop Proc. 6 (2019) 363–376.
- [61] M.L. Zamora, J. Rice, K. Koehler, One year evaluation of three low-cost PM_{2.5} monitors, *Atmos. Environ.* 235 (2020) 117615.
- [62] A. Ahmed, et al., Increased milk yield and reduced enteric methane concentration on a commercial dairy farm associated with dietary inclusion of sugarcane extract (*Saccharum officinarum*), *Animals* 13 (2023).
- [63] J.H. Bang, C.A. Santos, Y.M. Jo, Energy efficient treatment of indoor volatile organic compounds using a serial dielectric barrier discharge reactor, *Process Saf. Environ. Protect.* 153 (2021) 29–36.
- [64] A. Calisan, D. Uner, Diversifying Solar Fuels. *Solar Fuels* 137–159, John Wiley & Sons, Ltd, 2023, <https://doi.org/10.1002/9781119752097.ch4>.
- [65] I. Cohen, T. Rapaport, R.T. Berger, S. Rachmilevitch, The effects of elevated CO₂ and nitrogen nutrition on root dynamics, *Plant Sci.* 272 (2018) 294–300.
- [66] L. Spinelle, M. Gerboles, M.G. Villani, M. Alexandre, F. Bonavitaola, Field calibration of a cluster of low-cost commercially available sensors for air quality monitoring. Part B: NO, CO and CO₂, *Sens. Actuat. B Chem.* 238 (2017) 706–715.
- [67] M. Yarar, A. Bouziani, D. Uner, Pd as a reduction promoter for TiO₂: Oxygen and hydrogen transport at 2D and 3D Pd interfaces with TiO₂ monitored by TPR, operando ¹H NMR and CO oxidation studies, *Catal. Commun.* 174 (2023) 106580.
- [68] HORIBA. Portable automated measuring system PG-350 P-AMS. 1 Preprint at (2019).
- [69] M.M. Amaral, et al., In situ and operando infrared spectroscopy of battery systems: progress and opportunities, *J. Energy Chem.* 81 (2023) 472–491.
- [70] Protea. P2000 continuous emission monitoring (CEMS/AMS) process analyser. Preprint at (2019).
- [71] Protea. P2000 In-situ CEM. Preprint at <https://www.protea.ltd.uk/p2000-in-situ-cem> (2021).
- [72] Mcmillen, B. D. & Williams, K. New gas analyzer technologies enhance ease of use and reduce operating costs. 21–25 (2021).
- [73] Dräger. Dräger X-zone® 5500 area monitor. <https://www.draeger.com/Content/Documents/Products/x-zone-5500-pi-9046709-en-master.pdf>.
- [74] G.I. Janith, et al., Advances in surface plasmon resonance biosensors for medical diagnostics: An overview of recent developments and techniques, *J. Pharmaceut. Biomed. Anal. Open* 2 (2023) 100019.
- [75] D. Romanini, I. Ventrillard, G. Méjean, J. Morville, E. Kerstel, Introduction to cavity enhanced absorption spectroscopy. Cavity-Enhanced Spectroscopy and Sensing, Springer Berlin Heidelberg, Berlin, Heidelberg, 2014, pp. 1–60, https://doi.org/10.1007/978-3-642-40003-2_1. Gagliardi, G. & Loock, H.-P.
- [76] Biosensing instrument. SPRm200Series. https://biosensingusa.com/wp-content/uploads/2020/01/SPRm-200-Datasheet-20202EN.web_.pdf.
- [77] S. Ekgasit, C. Thammacharoen, F. Yu, W. Knoll, Influence of the metal film thickness on the sensitivity of surface plasmon resonance biosensors, *Appl. Spectrosc.* 59 (2005) 661–667.
- [78] E. Reimhult, C. Larsson, B. Kasemo, F. Höök, Simultaneous surface plasmon resonance and quartz crystal microbalance with dissipation monitoring measurements of biomolecular adsorption events involving structural transformations and variations in coupled water, *Anal. Chem.* 76 (2004) 7211–7220.
- [79] P. Ansorena, A. Zuzuarregui, E. Pérez-Lorenzo, M. Mujika, S. Arana, Comparative analysis of QCM and SPR techniques for the optimization of immobilization sequences, *Sens. Actuat. B Chem.* 155 (2011) 667–672.
- [80] Scientific Services. Photoacoustic gas monitor INNOVA 1412i. <https://scientificservices.eu/item/photoacoustic-gas-monitor-innova-1412i/759>.
- [81] ABB. Process analytics - infrared absorption. <https://shorturl.at/xNp6Y>.
- [82] A.A. Bunaciu, H.Y. Aboul-Enein, V.D. Raman Hoang, Spectroscopy for Protein Analysis, *Appl. Spectrosc. Rev.* 50 (2015) 377–386.
- [83] S.S. Chan, I.E. Wachs, L.L. Murrell, L. Wang, W.K. Hall, In situ laser Raman spectroscopy of supported metal oxides, *J. Phys. Chem.* 88 (1984) 5831–5835.
- [84] Ferraro, J. R., Nakamoto, K. & Brown, C. W. Introductory Raman spectroscopy: second edition. Introductory Raman spectroscopy: second edition (2003). doi:10.1016/B978-0-12-254105-6.X5000-8.
- [85] C.-C. Huang, Applications of Raman spectroscopy in herbal medicine, *Appl. Spectrosc. Rev.* 51 (2016) 1–11.
- [86] H. Lui, J. Zhao, D. McLean, H. Zeng, Real-time raman spectroscopy for in vivo skin cancer diagnosis, *Cancer Res.* 72 (2012) 2491–2500.
- [87] R.L. McCreery, Raman Spectroscopy for Chemical Analysis, John Wiley & Sons, 2005.
- [88] K. Nakamoto, Infrared and Raman Spectra of Inorganic and Coordination Compounds, Part B: Applications in Coordination, Organometallic, and Bioinorganic Chemistry, John Wiley & Sons, 2009.
- [89] R. Ramakrishnaiah, et al., Applications of Raman spectroscopy in dentistry: analysis of tooth structure, *Appl. Spectrosc. Rev.* 50 (2015) 332–350.
- [90] G.K. Ramesha, N.S. Sampath, Electrochemical reduction of oriented graphene oxide films: an in situ Raman spectroelectrochemical study, *J. Phys. Chem. C* 113 (2009) 7985–7989.
- [91] E. Smith, G. Dent, Modern Raman Spectroscopy: A Practical Approach, John Wiley & Sons, 2019.
- [92] M.A. Vuurman, I.E. Wachs, In situ Raman spectroscopy of alumina-supported metal oxide catalysts, *J. Phys. Chem.* 96 (1992) 5008–5016.
- [93] Renishaw. InVia™ research-grade confocal Raman microscopes. <https://shorturl.at/bBwqC>.
- [94] B&W Tek. New DIY Raman modules. <https://bwtek.com/diy-raman-modules/>.
- [95] G. Keresztury, Raman spectroscopy: theory. Handbook of Vibrational Spectroscopy, 2001, <https://doi.org/10.1002/0470027320.s0109>. Preprint at.
- [96] F.A. Bais, J.D. Farmer, The Physics of Information. Philosophy of Information, 8, Elsevier B.V., 2008.
- [97] R. Loudon, Time-reversal symmetry in light-scattering theory, *J. Raman Spectrosc.* 7 (1978) 10–14.
- [98] E.S. Yeung, M. Heiling, G.J. Small, Pre-resonance Raman intensities, *Spectrochim. Acta* 31 (1975) 1921–1931.
- [99] J. Aaltonen, K.C. Gordon, C.J. Strachan, T. Rades, Perspectives in the use of spectroscopy to characterise pharmaceutical solids, *Int. J. Pharm.* 364 (2008) 159–169.
- [100] J. Aaltonen, et al., Solid form screening - a review, *Eur. J. Pharmaceut. Biopharmaceut.* 71 (2009) 23–37.
- [101] G. Févotte, In situ Raman spectroscopy for in-line control of pharmaceutical crystallization and solids elaboration processes: a review, *Chem. Eng. Res. Des.* 85 (2007) 906–920.
- [102] I.M. Mills, Raman selection rules for vibration-rotation transitions in symmetric top molecules, *Mol. Phys.* 8 (1964) 363–373.
- [103] I. Nottingher, et al., In situ characterisation of living cells by Raman spectroscopy, *Spectroscopy* 16 (2002) 43–51.
- [104] W. Kiefer, The Raman Effect? A Unified Treatment of the Theory of Raman Scattering by Molecules, John Wiley & Sons, Ltd., 2002, p. 597. Derek A. Long ISBN 0-471-49028-8. Journal of Raman Spectroscopy 34, 180 (2003).
- [105] Bass, M., Stryland, E. Van, Williams, D. R. & Wolfe, W. L. Handbook of optics Vol IV. (2001).

- [106] Lahaye, T., Menotti, C., Santos, L., Lewenstein, M. & Pfau, T. The physics of dipolar bosonic quantum gases. (2009) doi:10.1088/0034-4885/72/12/126401.
- [107] D. Wolverson, Raman spectroscopy. Characterization of Semiconductor Heterostructures and Nanostructures, Elsevier, 2008, pp. 249–288.
- [108] P. Graves, D. Gardiner, Practical Raman Spectroscopy, Springer, 1989.
- [109] R.W. Boyd, Material slow light and structural slow light: similarities and differences for nonlinear optics [Invited], J. Optic. Soc. Am. B 28 (2011) A38.
- [110] R.C. Prince, R.R. Frontiera, E.O. Potma, Stimulated Raman scattering: from bulk to nano, Chem. Rev. 117 (2017) 5070–5094.
- [111] N. Bloembergen, The stimulated Raman effect, Am. J. Phys. 35 (1967) 989–1023.
- [112] J.B. Snow, S.-X. Qian, R.K. Chang, Stimulated Raman scattering from individual water and ethanol droplets at morphology-dependent resonances, Opt. Lett. 10 (1985) 37.
- [113] A. Zumbusch, G.R. Holtom, X.S. Xie, Three-dimensional vibrational imaging by coherent Anti-Stokes Raman scattering, Phys. Rev. Lett. 82 (1999) 4142–4145.
- [114] R.R. Jones, D.C. Hooper, L. Zhang, D. Wolverson, V.K. Raman Valev, Techniques: fundamentals and frontiers, Nanoscale Res. Lett. 14 (2019).
- [115] Cheng, J.-X. & Xie, X. S. Coherent Anti-Stokes Raman scattering microscopy: instrumentation, theory, and applications. (2004) doi:10.1021/jp035693v.
- [116] Bixler, J. N. Integrating cavity enhanced spectroscopy for liquid and gas sensing. in (2015).
- [117] T.Z. Moore, et al., Chemical, biological, and trace gas detection and measurement with a newly developed integrating Cavity Enhanced Raman (iCERS) technique, *Comm. + Sci. Sens. Imaging* (2018).
- [118] T.Z. Moore, et al., Integrating cavity enhanced Raman spectroscopy of trace gases and bulk compounds, in: *Conference on Lasers and Electro-Optics JTh2A.87, OSA, 2019*, https://doi.org/10.1364/CLEO_AT.2019.JTh2A.87.
- [119] P. Wang, W. Chen, F. Wan, J. Wang, J. Hu, A review of cavity-enhanced Raman spectroscopy as a gas sensing method, *Appl. Spectrosc. Rev.* 55 (2020) 393–417.
- [120] N. Djaker, D. Gachet, N. Sandeau, P.-F. Lenne, H. Rigneault, Refractive effects in coherent anti-Stokes Raman scattering microscopy, *Appl. Opt.* 45 (2006) 7005.
- [121] Campion, A. & Kambhampati, P. Surface-enhanced Raman scattering.
- [122] BRAVO Handheld Raman Spectrometer - Bruker.
- [123] J.-F. Tomb, et al., Enhanced Raman.pdf, *Nature* 388 (1997) 539–547. Preprint at.
- [124] Beyond the diffraction limit, *Nat. Photonics.* 3 (2009) 361.
- [125] N. Kumar, B.M. Weckhuysen, A.J. Wain, A.J. Pollard, Nanoscale chemical imaging using tip-enhanced Raman spectroscopy, *Nat. Protoc.* 14 (2019) 1169–1193.
- [126] E.M. van Schroyen Lantman, T. Deckert-Gaudig, A.J.G. Mank, V. Deckert, B. M. Weckhuysen, Catalytic processes monitored at the nanoscale with tip-enhanced Raman spectroscopy, *Nat. Nanotechnol.* 7 (2012) 583–586.
- [127] H.A. Hyatt, J.M. Cherlow, W.R. Fenner, S.P.S. Porto, Cross section for the Raman effect in molecular nitrogen gas, *J. Opt. Soc. Am.* 63 (1973) 1604.
- [128] Buric, M. P. Gas phase Raman spectroscopy using hollow waveguides. (2010).
- [129] A.S. Hicilyilmaz, A.C. Bedeloglu, Applications of polyimide coatings: a review, *SN Appl. Sci.* 3 (2021) 1–22.
- [130] M.P. Buric, K.P. Chen, J. Falk, S.D. Woodruff, Enhanced spontaneous Raman scattering and gas composition analysis using a photonic crystal fiber, *Appl. Opt.* 47 (2008) 4255–4261.
- [131] M.P. Buric, K.P. Chen, J. Falk, S.D. Woodruff, Improved sensitivity gas detection by spontaneous Raman scattering, *Appl. Opt.* 48 (2009) 4424.
- [132] J. Kiefer, et al., Design and characterization of a Raman-scattering-based sensor system for temporally resolved gas analysis and its application in a gas turbine power plant, *Meas. Sci. Technol.* 19 (2008).
- [133] S.N. White, Laser Raman spectroscopic analyses of dissolved gases, 3–8 Preprint at (2007).
- [134] E.T.M. Dlugosz, et al., Filament-assisted impulsive Raman spectroscopy of ozone and nitrogen oxides, *J. Phys. Chem. A* 119 (2015) 9272–9280.
- [135] S. Hanf, R. Keiner, D. Yan, J. Popp, T. Frosch, Fiber-enhanced Raman multigas spectroscopy: a versatile tool for environmental gas sensing and breath analysis, *Anal. Chem.* 86 (2014) 5278–5285.
- [136] R.L. Aggarwal, L.W. Farrar, S.Di Cecca, T.H. Jeys, Raman spectra and cross sections of ammonia, chlorine, hydrogen sulfide, phosgene, and sulfur dioxide toxic gases in the fingerprint region 400–1400 cm⁻¹, *AIP. Adv.* 6 (2016) 1–7.
- [137] Y. Fan, C.J. Cornelius, Raman spectroscopic and gas transport study of a pentablock ionomer complexed with metal ions and its relationship to physical properties, *J. Mater. Sci.* 48 (2013) 1153–1161.
- [138] Y.V. Fedoseeva, et al., Effect of hydrogen fluoride addition and synthesis temperature on the structure of double-walled carbon nanotubes fluorinated by molecular fluorine, *Phys. Status Solidi (B)* 255 (2018) 1700261.
- [139] R.A. Cleis, W.B. Roh, L.P. Goss, Raman linewidths of hydrogen fluoride determined by using low-resolution coherent anti-Stokes Raman spectroscopy, *J. Optic. Soc. America B* 1 (1984) 774–778.
- [140] T. Jochum, B. Michalzik, A. Bachmann, J. Popp, T. Frosch, Microbial respiration and natural attenuation of benzene contaminated soils investigated by cavity enhanced Raman multi-gas spectroscopy, *Analyst* 140 (2015) 3143–3149.
- [141] P. Borowski, W. Gac, P. Pulay, K. Woliński, The vibrational spectrum of 1,4-dioxane in aqueous solution-theory and experiment, *N. J. Chem.* 40 (2016) 7663–7670.
- [142] T. Kim, R.S. Assary, L.A. Curtiss, C.L. Marshall, P.C. Stair, Vibrational properties of levulinic acid and furan derivatives: Raman spectroscopy and theoretical calculations, *J. Raman Spectrosc.* 42 (2011) 2069–2076.
- [143] J. Cheng, P. Wang, X. Su, Recent progress on the detection of dioxins based on surface-enhanced Raman spectroscopy, *Acta Chim. Sin.* 77 (2019) 977–983.
- [144] M. Hippler, Cavity-enhanced Raman spectroscopy of natural gas with optical feedback cw-diode lasers, *Anal. Chem.* 87 (2015) 7803–7809.
- [145] W.F. Murphy, W. Holzer, H.J. Bernstein, Gas phase Raman intensities: a review of 'pre-laser' data, *Appl. Spectrosc.* 23 (1969) 211–218.
- [146] Drysdale, C. Combining chemistry and artistry: synthesis and identification of artistic copper patinas using Raman spectroscopy. 1, (2014).
- [147] V. Hayez, V. Costa, J. Guillaume, H. Terryn, A. Hubin, Micro Raman spectroscopy used for the study of corrosion products on copper alloys: study of the chemical composition of artificial patinas used for restoration purposes, *Analyst* 130 (2005) 550–556.
- [148] S.A. V. Y. Ruan, S.C. Warren-Smith, T.M. Monro, Enhanced fluorescence sensing using microstructured optical fibers: a comparison of forward and backward collection modes, *Opt. Lett.* 33 (2008) 1473.
- [149] R. Chen, et al., Photonic Bandgap Fiber-Enabled Raman Detection of Nitrogen Gas, 7322, *SPIE*, 2009, <https://doi.org/10.1117/12.817823> eds. Xiao, H., Fan, X. & Wang, A.73220N.
- [150] C. Wang, A. Mbi, M. Shepherd, A study on breath acetone in diabetic patients using a cavity ringdown breath analyzer: exploring correlations of breath acetone with blood glucose and glycohemoglobin A1C, *IEEe Sens. J.* 10 (2010) 54–63.
- [151] K.K. Chow, M. Short, S. Lam, A. McWilliams, H. Zeng, A Raman cell based on hollow core photonic crystal fiber for human breath analysis, *Med. Phys.* 41 (2014) 92701.
- [152] A. Lambrecht, et al., Neue Methoden der laserbasierten Gasanalytik, *Chem. Ing. Tech.* 88 (2016) 746–755.
- [153] Wolf, S., Frosch, T., Popp, J., Pletz, M. W. & Frosch, T. molecules highly sensitive detection of the antibiotic ciprofloxacin by means of fiber enhanced Raman spectroscopy. (2019) doi:10.3390/molecules24244512.
- [154] W.S.M. Brooks, et al., Development of a gas-phase Raman instrument using a hollow core anti-resonant tubular fibre, *J. Raman Spectrosc.* 52 (2021) 1772–1782.
- [155] G.T. Jasion, et al., Fabrication of tubular anti-resonant hollow core fibers: modelling, draw dynamics and process optimization, *Opt. Express.* 27 (2019) 20567.
- [156] Y. Bai, D. Xiong, Z. Yao, X. Wang, D. Zuo, Analysis of CH₄, C₂H₆, C₂H₄, C₂H₂, H₂, CO, and H₂S by forward Raman scattering with a hollow-core anti-resonant fiber, *J. Raman Spectrosc.* 53 (2022) 1023–1031.
- [157] F. Hu, L. Shi, W. Min, Biological imaging of chemical bonds by stimulated Raman scattering microscopy, *Nat. Methods* 16 (2019) 830–842.
- [158] F. Yang, W. Jin, All-fiber hydrogen sensor based on stimulated Raman gain spectroscopy with a 1550-nm hollow-core fiber, in: 25th International Conference on Optical Fiber Sensors 10323, 2017 103233C.
- [159] Q. Cheng, Y. Miao, J. Wild, W. Min, Y. Yang, Emerging applications of stimulated Raman scattering microscopy in materials science, in: *Matter*, 4, Cell Press, 2021, pp. 1460–1483.
- [160] W. Min, C.W. Freudiger, S. Lu, X.S. Xie, Coherent nonlinear optical imaging: beyond fluorescence microscopy, *Annu. Rev. Phys. Chem.* 62 (2011) 507–530.
- [161] C.W. Freudiger, et al., Label-free biomedical imaging with high sensitivity by stimulated Raman scattering microscopy, *Science* (1979) 322 (2008) 1857–1861.
- [162] G. Fleury, et al., Resolving the framework position of organic structure-directing agents in hierarchical zeolites via polarized stimulated Raman scattering, *J. Phys. Chem. Lett.* 9 (2018) 1778–1782.
- [163] L.M. Malard, et al., Studying 2D materials with advanced Raman spectroscopy: CARS, SRS and TERS, *Phys. Chem. Chem. Phys.* 23 (2021) 23428–23444.
- [164] Y. Ozeki, et al., High-speed molecular spectral imaging of tissue with stimulated Raman scattering, *Nat. Photonics.* 6 (2012) 845–851.
- [165] C.H. Camp, M.T. Cicerone, Chemically sensitive bioimaging with coherent Raman scattering, *Nat. Photonics.* 9 (2015) 295–305.
- [166] Y. Bi, et al., Near-resonance enhanced label-free stimulated Raman scattering microscopy with spatial resolution near 130 nm, *Light. Sci. Appl.* 7 (2018) 81.
- [167] P.N. Malevich, et al., Ultrafast-laser-induced backward stimulated Raman scattering for tracing atmospheric gases, *Opt. Express.* 20 (2012) 18784–18794.
- [168] P.N. Malevich, et al., Stimulated Raman gas sensing by backward UV lasing from a femtosecond filament, *Opt. Lett.* 40 (2015) 2469–2472.
- [169] R.W. Maker, D. P. Terhune, Study of optical effects due to an induced polarization third order in the electrical field strength, *Phys. Rev.* 137 (1965) A801–A818.
- [170] R.F. Begley, A.B. Harvey, R.L. Byer, Coherent Anti-Stokes Raman spectroscopy, *Appl. Phys. Lett.* 25 (1974) 387–390.
- [171] M.D. Duncan, J. Reintjes, T.J. Manuccia, Scanning coherent anti-Stokes Raman microscope, *Opt. Lett.* 7 (1982) 350–352.
- [172] C.L. Evans, X.S. Xie, Coherent Anti-Stokes Raman scattering microscopy: chemical imaging for biology and medicine, *Annu. Rev. Anal. Chem.* 1 (2008) 883–909.
- [173] R.M. Goodhead, J. Moger, T.S. Galloway, C.R. Tyler, Tracing engineered nanomaterials in biological tissues using coherent anti-Stokes Raman scattering (CARS) microscopy – A critical review, *Nanotoxicology.* 9 (2015) 928–939.
- [174] S. Roy, J.R. Gord, A.K. Patnaik, Recent advances in coherent anti-Stokes Raman scattering spectroscopy: Fundamental developments and applications in reacting flows, *Prog. Energy Combust. Sci.* 36 (2010) 280–306.
- [175] C. Hess, New advances in using Raman spectroscopy for the characterization of catalysts and catalytic reactions, *Chem. Soc. Rev.* 50 (2021) 3519–3564.
- [176] S. Zaitzu, T. Imasaka, Intracavity phase-matched coherent Anti-Stokes Raman spectroscopy for trace gas detection, *Anal. Sci.* 30 (2013) 75–79.
- [177] T.R. Meyer, S. Roy, J.R. Gord, Improving signal-to-interference ratio in rich hydrocarbon-air flames using picosecond coherent anti-stokes Raman scattering, *Appl. Spectrosc.* 61 (2007) 1135–1140.
- [178] S. Sugimoto, I. Asahi, T. Shiina, A practical-use hydrogen gas leak detector using CARS, *Int. J. Hydrog. Energy* 46 (2021).

- [179] A. Bohlin, C.J. Kiewer, Communication: Two-dimensional gas-phase coherent anti-Stokes Raman spectroscopy (2D-CARS): simultaneous planar imaging and multiplex spectroscopy in a single laser shot, *J. Chem. Phys.* 138 (2013).
- [180] J. Langer, et al., Present and Future of Surface-Enhanced Raman Scattering, *ACS. Nano* 14 (2020) 28–117.
- [181] X. Qiao, et al., Selective surface enhanced Raman scattering for quantitative detection of lung cancer biomarkers in superparticle@MOF structure, *Adv. Mater.* 30 (2018).
- [182] B. Sharma, R.R. Frontiera, A.I. Henry, E. Ringe, R.P. Van Duyne, SERS: materials, applications, and the future, *Mater. Today* 15 (2012) 16–25.
- [183] G.C. Schatz, M.A. Young, R.P. Van Duyne, Electromagnetic mechanism of SERS, *Top. Appl. Phys.* 103 (2006) 19–46.
- [184] K.A. Willets, Surface-enhanced Raman scattering (SERS) for probing internal cellular structure and dynamics, *Anal. Bioanal. Chem.* 394 (2009) 85–94.
- [185] A. Otto, The ‘chemical’ (electronic) contribution to surface-enhanced Raman scattering, *J. Raman Spectrosc.* 36 (2005) 497–509.
- [186] Xie, X., Pu, H. & Sun, D.-W. Critical reviews in food science and nutrition recent advances in nanofabrication techniques for SERS substrates and their applications in food safety analysis recent advances in nanofabrication techniques for SERS substrates and their applications in foo. (2017) doi:10.1080/10408398.2017.1341866.
- [187] C.L. Wong, U.S. Dinish, M.S. Schmidt, M. Olivo, Non-labeling multiplex surface enhanced Raman scattering (SERS) detection of volatile organic compounds (VOCs), *Anal. Chim. Acta* 844 (2014) 54–60.
- [188] R.K. Lauridsen, et al., SERS spectroscopy for detection of hydrogen cyanide in breath from children colonised with *P. aeruginosa*, *Anal. Methods* 9 (2017) 5757–5762.
- [189] L. Chen, H. Guo, F. Sassa, B. Chen, K. Hayashi, Sers gas sensors based on multiple polymer films with high design flexibility for gas recognition, *Sensors* 21 (2021) 1–13.
- [190] G. Peng, et al., Diagnosing lung cancer in exhaled breath using gold nanoparticles, *Nat. Nanotechnol.* (2009), <https://doi.org/10.1038/NNANO.2009.235>.
- [191] N. Shehata, et al., Silicon nanowire sensors enable diagnosis of patients via exhaled breath, *ACS. Nano* 10 (2016) 7047–7057.
- [192] Z. Zhang, et al., Ultrasensitive surface-enhanced Raman scattering sensor of gaseous aldehydes as biomarkers of lung cancer on dendritic Ag nanocrystals, *Anal. Chem.* 89 (2017) 1416–1420.
- [193] K. Fiederling, S. Kupfer, S. Gräfe, Are charged tips driving TERS-resolution? A full quantum chemical approach, *J. Chem. Phys.* 154 (2021).
- [194] Y. Cao, M. Sun, Tip-enhanced Raman spectroscopy, *Rev. Phys.* 8 (2022) 100067.
- [195] Z. Yang, J. Aizpurua, H. Xu, Electromagnetic field enhancement in TERS configurations, *J. Raman Spectrosc.* 40 (2009) 1343–1348.
- [196] K.D. Park, M.B. Raschke, J.M. Atkin, Y.H. Lee, M.S. Jeong, Probing bilayer grain boundaries in large-area graphene with tip-enhanced Raman spectroscopy, *Adv. Mater.* 29 (2017).
- [197] S. Sheng, et al., Vibrational properties of a monolayer silicene sheet studied by tip-enhanced Raman spectroscopy, *Phys. Rev. Lett.* 119 (2017) 196803.
- [198] D. Kuroski, Advances of tip-enhanced Raman spectroscopy (TERS) in electrochemistry, biochemistry, and surface science, *Vib. Spectrosc.* 91 (2017) 3–15.
- [199] R. Treffer, et al., Advances in TERS (tip-enhanced Raman scattering) for biochemical applications, *Biochem. Soc. Trans.* 40 (2012) 609–614.
- [200] D. Cialla, et al., Raman to the limit: tip-enhanced Raman spectroscopic investigations of a single tobacco mosaic virus, *J. Raman Spectrosc.* 40 (2009) 240–243.
- [201] C. Gullekson, L. Lucas, K. Hewitt, L. Kreplak, Surface-sensitive Raman spectroscopy of collagen I fibrils, *Biophys. J.* 100 (2011) 1837–1845.
- [202] Z. He, et al., Tip-enhanced Raman imaging of single-stranded DNA with single base resolution, *J. Am. Chem. Soc.* 141 (2019) 753–757.
- [203] D. Kuroski, M. Mattei, R.P. Van Duyne, Probing redox reactions at the nanoscale with electrochemical tip-enhanced Raman spectroscopy, *Nano Lett.* 15 (2015) 7956–7962.
- [204] T.-X. Huang, et al., Tip-enhanced Raman spectroscopy: tip-related issues, *Anal. Bioanal. Chem.* 407 (2015) 8177–8195.
- [205] D. Kuroski, S. Zaleski, F. Casadio, R.P. Van Duyne, N.C. Shah, Tip-enhanced Raman spectroscopy (TERS) for in situ identification of indigo and iron gall ink on paper, *J. Am. Chem. Soc.* 136 (2014) 8677–8684.
- [206] P. Singh, et al., Differences in single and aggregated nanoparticle plasmon spectroscopy, *Phys. Chem. Chem. Phys.* 17 (2015) 2991–2995.
- [207] J.M. Klingsporn, et al., Intramolecular insight into adsorbate–substrate interactions via low-temperature, ultrahigh-vacuum tip-enhanced Raman spectroscopy, *J. Am. Chem. Soc.* 136 (2014) 3881–3887.
- [208] Z. Liu, et al., Revealing the molecular structure of single-molecule junctions in different conductance states by fishing-mode tip-enhanced Raman spectroscopy, *Nat. Commun.* 2 (2011) 305.
- [209] N. Jiang, et al., Tip-enhanced Raman spectroscopy: From concepts to practical applications, *Chem. Phys. Lett.* 659 (2016) 16–24.
- [210] S. Schlüter, N. Popovska-Leipertz, T. Seeger, A. Leipertz, Gas sensor for volatile anesthetic agents based on Raman scattering, *Physics Procedia*, 2012, <https://doi.org/10.1016/j.phpro.2012.10.108>.
- [211] Materials, A. Z. O. & tec5USA Inc. Using in - line Raman spectroscopy for natural gas monitoring online analysis with Raman spectroscopy. 1–9 (2021).
- [212] A. Sieburg, S. Schneider, D. Yan, J. Popp, T. Frosch, Monitoring of gas composition in a laboratory biogas plant using cavity enhanced Raman spectroscopy, *Analyst* 143 (2018) 1358–1366.
- [213] S.B. Hansen, The application of Raman spectroscopy for analysis of multi-component systems, *Techn. Univ. Denmark* 167 (2000).
- [214] for Standardization, I. O., ISO 23978:2020(en) natural gas — upstream area — determination of composition by Laser Raman spectroscopy, *ISO 1* (2020) 20. Preprint at.
- [215] Insight, O. Raman solutions. 2 Preprint at [https://www.oceaninsight.com/products/spectrometers/raman/\(2022\)](https://www.oceaninsight.com/products/spectrometers/raman/(2022)).
- [216] Chapter 12 - the molecule in an electric or magnetic field, *Ideas of Quantum Chemistry*, Elsevier, 2007, pp. 615–680, <https://doi.org/10.1016/B978-044452227-6/50013-2>. Piel, L.
- [217] R.P. Ozerov, A.A. Vorobyev, Dielectric properties of substances, *Phys. Chemists* (2007) 251–304, <https://doi.org/10.1016/B978-044452830-8/50006-4>.
- [218] A.H. Harvey, E.W. Lemmon, Method for estimating the dielectric constant of natural gas mixtures 1, *Int. J. Thermophys.* 26 (2005).
- [219] J. Clark, What causes molecules to absorb UV and visible light, *Truro School Cornwall* (2020) 1–8.
- [220] Y. Wan, et al., Manipulating the Raman scattering rotation: via magnetic field in an MoS₂ monolayer, *RSC. Adv.* 11 (2021) 4035–4041.
- [221] G.A. Ozin, Gas-phase Raman spectroscopy. The vibrational spectra (infrared and Raman) of hexachlorodisilane (gas, liquid, and solid) and assignment of fundamentals, *J. Chem. Soc. A* (1969) 2952–2954, <https://doi.org/10.1039/J19690002952>.
- [222] T.F. Morse, Kinetic model for gases with internal degrees of freedom, *Phys. Fluids* 7 (1964) 159–169, <https://doi.org/10.1063/1.1711128>. Preprint at.
- [223] Woit, P. Quantum theory, groups and representations: an introduction revised and expanded version, under construction. (2020).
- [224] S.Y. Lee, Placzek-type polarizability tensors for Raman and resonance Raman scattering, *J. Chem. Phys.* 78 (1982) 723–734.
- [225] L. Pitre, M.D. Plimmer, F. Sparasci, M.E. Himbert, Determinations of the Boltzmann constant, *C. R. Phys.* 20 (2019) 129–139.
- [226] Biedrzycki, S. Advanced techniques for gas-phase Raman spectroscopy. 1–88 (2011).